

Development of an indole-amide-based photoswitchable cannabinoid receptor subtype 1 (CB₁R) “cis-on” agonist

Diego A. Rodríguez-Soacha[§], Sophie A. M. Steinmüller[§], Ali İşbilir^{ψ, ‡}, Julia Fender^ψ, Marie H. Deventer^φ, Yesid A. Ramírez^{§, †}, Anna Tutov[§], Christoph Sottriffer[§], Christophe P. Stove^φ, Kristina Lorenz^{ψ, ○}, Martin J. Lohse^{ψ, ‡}, James N. Hislop^l, Michael Decker^{*, §}

[§]Pharmazeutische und Medizinische Chemie, Institut für Pharmazie und Lebensmittelchemie, Julius-Maximilians-Universität Würzburg, Am Hubland, 97074 Würzburg, Germany.

^ψInstitut für Pharmakologie und Toxikologie, Julius-Maximilians-Universität Würzburg, Versbacher Str. 9 D-97078 Würzburg, Germany.

[‡]Receptor Signaling Group, Max Delbrück Center for Molecular Medicine, 13125 Berlin, Germany.

^φLaboratory of Toxicology, Department of Bioanalysis, Faculty of Pharmaceutical Sciences, Ghent University, Otergemsesteenweg 460, 9000 Ghent, Belgium.

[†]Departamento de Ciencias Farmacéuticas, Facultad de Ciencias Naturales, Universidad Icesi, Valle del Cauca 760031, Cali, Colombia.

[○]Leibniz-Institut für Analytische Wissenschaften – ISAS e.V., Bunsen-Kirchhoff-Str. 11, 44139 Dortmund, Germany.

^lSchool of Medicine, Medical Sciences and Nutrition, Institute of Medical Sciences, University of Aberdeen, Foresterhill, Aberdeen AB25 2ZD, United Kingdom

KEYWORDS photopharmacology, CB₁ agonist, G protein-coupled receptor, diazocine, photo-rimonabant, optical control.

ABSTRACT: Activation of the human cannabinoid receptor type 1 (*hCB₁R*) with high spatiotemporal control is useful to study processes involved in different pathologies related to nociception, metabolic alterations and neurological disorders. To synthesize new agonist ligands for *hCB₁R*, we have designed different classes of photoswitchable molecules based on an indole core. The modifications made to the central core have allowed us to understand the molecular characteristics necessary to design an agonist with optimal pharmacological properties. Compound **27a** shows high affinity for CB₁R (K_i (*cis* form) = 0.18 μM), with a marked difference in affinity with respect to its inactive “*trans-off*” form (CB₁R K_i *trans/cis* ratio = 5.4). The novel compounds were evaluated by radioligand binding studies, receptor internalization, sensor receptor activation (GRABeCB2.0), and calcium mobilization assays. The data shows that the novel agonist **27a** is a candidate for studying of the optical modulation of CBRs, serving as a new molecular tool for investigating the involvement of *hCB₁R* in disorders associated with the endocannabinoid system.

INTRODUCTION

In 1964 Gaoni and Mechoulam first identified Δ¹-3,4-*trans*-tetrahydrocannabinol as an active component from *Cannabis sativa L.* which was the vital first step in understanding the endocannabinoid system.¹ From there, as a result of multiple investigations, it was possible to identify the two canonical cannabinoid receptors reported to date, named as human cannabinoid receptor type 1 (*hCB₁R*) and type 2 (*hCB₂R*).^{2,3} Although both receptors share characteristics at the structural level, the distribution of the tissues where they are expressed, as well as the differences in the transduction systems makes the clinical relevance between both receptors differ.²⁻⁵

Specifically, CB₁R agonist ligands have great clinical relevance in the treatment of various pathologies. In studies with knockout animals, it has been found that the administration of CB₁R agonists causes a decrease in depressive and anxiety-like behaviors, whose biological effect is abolished by the administration of CB₁R antagonists.^{6,7} Similarly, by activating CB₁R in murine epilepsy models, it has been possible to reduce the intensity of seizures, suggesting that these agonists may be beneficial for patients with treatment-resistant epilepsy.⁸ Another aspect of clinical relevance is weight control, where CB₁R agonists have been shown to be useful in treating of certain metabolic disorders. CB₁R activation induces an antiemetic and satiety-inhibiting effect, which generates a positive energy mainte-

nance effect by increasing food intake and, therefore, increasing body weight. These effects are beneficial for the treatment of metabolic disorders such as cachexia and anorexia generated in patients with underlying pathologies such as cancer, HIV/AIDS or Alzheimer's disease.⁹⁻¹² Additionally, the antinociceptive effects produced by CB₁R agonist ligands in both inflammatory and neuropathic pain models open the possibility of new types of treatments with fewer adverse effects for patients with chronic disabling diseases.¹³

Despite having multiple therapeutic uses, some CB₁R agonists are sold on the black market for their recreational effects, being used to induce hallucinogenic and relaxing effects, as well as substances with the potential to "increase creativity".^{14,15} However, its misuse can lead to multiple adverse effects, especially when consumed in excess. It has been documented that intoxication can produce a variety of cardiotoxic, psychiatric and neurological effects, as well as develop a certain degree of dependence in some individuals.¹⁶

All these biological effects have led to the need for a more detailed exploration of CB₁R, so that through new ligands designed as molecular tools, the receptor activation mechanism can be understood in detail at both central and peripheral levels. Molecular tool compounds are useful substances in the study of molecular biology and medicinal chemistry. These molecules allow analyzing the signaling networks, and the biological effect given by the interaction with the receptor in a specific tissue or organ in a spatiotemporal manner.¹⁷ To achieve this specificity, it is necessary to use various external stimuli to generate the release or activation of the ligand directly in the selected tissue.¹⁸ Many of the new molecular tools designed to study the nature of biological receptors have the disadvantage of generating irreversible type reactions (for example, controlled release systems through hydrolysis of molecular bonds). In this way, although it is possible to activate the receptor in a precise temporal-spatial way, it is not possible to return to the initial state spontaneously. To solve this, new ligands have been designed which can function as molecular switches in such a way that they can activate or deactivate the receptor through the use of external light sources.¹⁹ When irradiated at specific wavelengths, these photo-ligands can isomerize in such a way that they can go from an inactivated "off" form to an active "on" photo-isomer, generating precise time-control of the biological activity of the receptor.¹⁹⁻²¹

The use of photo-pharmacological tools for the exploration of receptors framed within complex pathologies is a topic of growing interest.^{22,23} Specifically for the hCB₁R, novel photoswitchable molecules designed for the study of the biological activity of the endocannabinoid system have been reported. By coupling Δ^9 -THC scaffold with an azobenzene moiety, Trauner, Carreira and coworkers designed two photoswitchable ligands with high affinity for CBRs.²⁴ These novel molecules allowed spatiotemporal control of CB₁R and its signaling pathways by isomerization with external light sources. Although the molecules derived from Δ^9 -THC are pioneers in the photopharmacological study of CBRs, however, like its parent compound, they could be non-selective toward other biological targets.²⁵ Such potentially pro-

miscuous ligands can give rise to undesirable adverse effects derived from the non-specific interaction with a variety of targets. To improve its specificity, in previous work by our research group, new photoligands derived from the benzimidazole core were synthesized. These partial agonist ligands showed a pronounced selectivity for CB₂R over CB₁R, having higher affinity in its *cis* photo-isomer.²⁶ Subsequently, Carreira, Frank and coworkers described the synthesis of highly selective CB₂R agonists coupled to fluorescent and photoswitchable moieties. This new class of hybrid photo-ligands has the ability to monitor CB₂R signaling by controlling calcium release in real time.^{27,28} Recently, Tao *et al.* have described the design of azoesters derived from the pharmacophoric structure of the CB₂R antagonist AM10257.²⁹ Using rational remodeling approach, they replaced the adamantyl group of the parent compound with an azobenzene moiety, thereby creating a new photoligand with an affinity for CB₂R in its *cis* form more than 40 times higher than its *trans* form. These results opened up new possibilities for photoligand design through a novel structure-guided approach.

In a recent work of our research group, we describe the synthesis of "photo-rimonabant" as a novel ligand designed from the rimonabant pharmacophore, substituting one of the pyrazole side arms for an azobenzene moiety by means of azo-extension techniques.³⁰ As a result, we obtained an antagonist with high selectivity for CB₁R over CB₂R and 15-fold higher affinity in its *cis* photo-isomer compared to the *trans* isomer.

For the present work, we wanted to design novel photoswitchable compounds with agonist activity on CB₁R. Although derivatives of Δ^9 -THC were previously reported in the literature,²⁴ in our group we wanted to focus on compounds derived on the indole core. The advantage of this core is that the target molecules are smaller and easier to synthesize. The synthesized compounds were photocharacterized and tested in different biological assays, validating the differences between their two isoforms of the most representative compounds with an amide bridge at C-3.

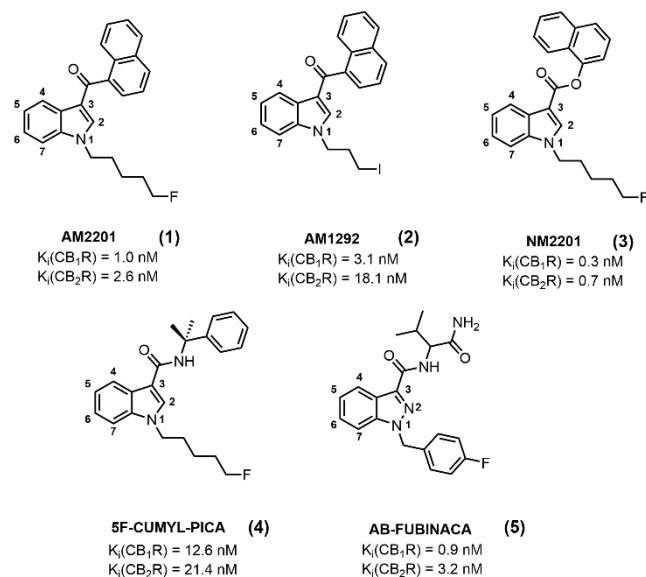
RESULTS AND DISCUSSION

Chemistry. For the design of the CB₁R agonist compounds, the structures of promising substances previously described in the literature were considered (**Chart 1**).^{14, 31-34} Within these substances, both the indole and indazole are the most common aromatic systems used as central core, which are substituted at the C-3 and N-1 positions with hydrophobic groups. Regarding N-1 substitutions, short aliphatic chains with 3-5 carbon atoms are usually attached, which may contain a halogen atom in their distal position, however, other hydrophobic substituents - more voluminous- are equally accepted.¹⁴ The substitution at C-3 usually occurs with bulky moieties such as naphthyl, benzyl or adamantyl, which are attached to the indole by a carbonyl linker, usually a ketone or amide bridge. This is because the carbonyl group is essential, generating hydrophilic interactions in one domain of the ligand binding pocket of CB₁R.³⁵ In view of the highly hydrophobic nature of CB₁R, it was decided to functionalize the central indole ring by attaching a moiety capable of isomerization by light. The chosen photoisomerizable group was azobenzene, due to its structural

characteristics that simulate common bulky groups such as naphthoyl. Additionally, azobenzenes are stable over a wide pH range and are usually easy to synthesize.³⁶⁻³⁸

Although agonist CB₁R photo-ligands based on the structure of THC have been previously reported in the literature.²⁴ In this project we decided to synthesize new cannabimimetic photoswitchable ligands core-based on the indole ring. These new photo-compounds are “small” and much easier to synthesize. Similarly, its relatively simple structure may enable higher selectivity for CB₁R.

Chart 1. Similarities found in CB₁ agonist molecules described in the literature.^{14, 31-34}

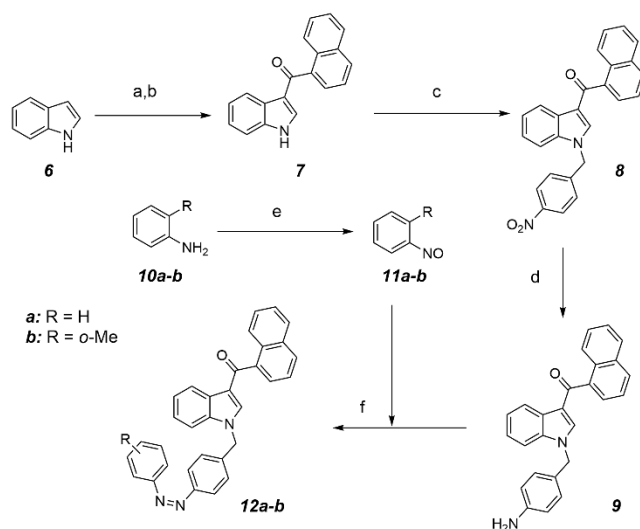


The first class of CB₁R ligands was designed by introducing different hydrophobic substituents at positions *N*-1 and *C*-3 of the central indole ring. First, to preserve the naphthoyl group in position *C*-3 starting from the pharmacophoric structure of reference compounds **1** and **2**. We decided to modify only the lateral aliphatic chain, attaching the azobenzene moiety to *N*-1 (**Scheme 1**). For this purpose, acylation of unsubstituted indole (**6**) was carried out by addition of Grignard reagent and 1-naphthoyl chloride, followed by a selective hydrolysis to yield intermediate **7**. By alkylation of compound **7** in position *N*-1, through the reaction with NaH and 1-bromo-4-nitrobenzene, intermediate **8** was obtained. Then, the nitro group was subsequently reduced to its respective amine **9** by hydrogenation. In parallel, aromatic amines **10a-b** were partially oxidized with MPS to generate the corresponding nitroso compounds **11a-b**. The mixture of the nitroso derivatives and intermediate **9** in acid conditions yielded the target compounds **12a-b** in moderate yields.

To compare the influence of the photoswitchable azobenzene at the different positions of the central ring, the following classes of compounds were designed to incorporate azobenzenes at position *C*-3 of the indole. As a first approach (**Scheme 2**), the indole **6** was reacted with substituted nitrobenzoylchloride - in *para* (**13a**), *meta* (**13b**) and *ortho* (**13c**) positions - in the presence of Grignard reagent at -

78°C. The yield of this reaction was highly dependent on substitution of the nitro group: substitution in *ortho*-position did not generate the desired product, but mainly a by-product corresponding to the alkylation of *N*-1. Substitution in *meta*-position gave low yields, with an overall value of 10% for compound **15b** after hydrolysis. On the other hand, substitution in *para*-position generated the best results, obtaining compound **15a** with an overall yield of 53%. Later, by deprotonation of the nitrogen with NaH, the aliphatic chain was incorporated into the intermediates to yield molecules **16a-b**. The nitro-compounds **16a-b** were hydrogenated to obtain the respective anilines **17a-b**. As a final step, the Baeyer-Mills reaction in acidic medium was performed to obtain the final compounds with substitution in *para* (**18**) and *meta* (**19a-b**) positions.

Scheme 1. Synthesis of photo-CB₁R ligands with introduction of azobenzene in position *N*-1.^a



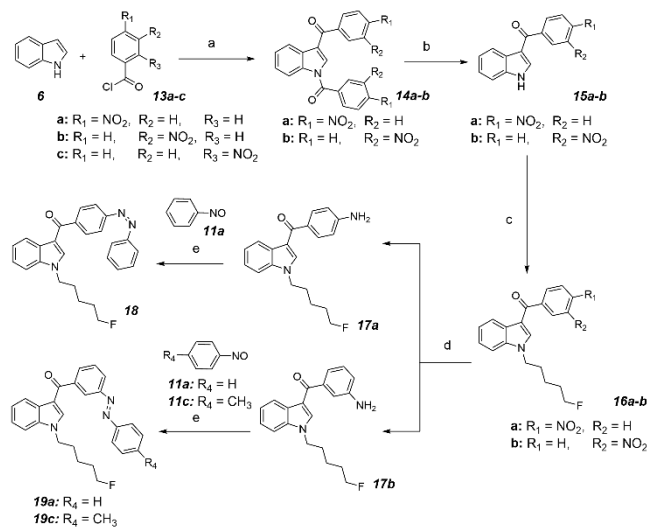
^aReagents and conditions: (a) MeMgBr, 1-naphthoylchloride, THF, -78°C, 4h; (b) LiOH, MeOH, THF, rt, 2h, 56%; (c) 1-bromo-4-nitrobenzene, NaH, DMF, 65°C, 3h, 58%; (d) H₂, Pd/C, EtOH, rt, 2h, 60%; (e) MPS, DCM/H₂O, rt, overnight; (f) AcOH/TFA/toluene, rt, overnight, 19-26%.

The second approach to synthesize substituted indoles with the azobenzene moiety in position *C*-3, was planned by replacing the ketone bridge with an amide bridge, like the pharmacophores in reference molecules **4** and **5** (**Figure 1, Scheme 3**). We also considered our previous experience regarding the synthesis of both CB₁R antagonists' photo-ligands as well as CB₂R photoswitchable agonists, where slight changes in aromatic substitution of the azobenzene moiety, could translate into large differences in affinity between the different structural isomers.^{26, 30} To evaluate the aromatic substitution, the synthesis proceeded by starting with amino-substituted aminobenzylamines at *ortho* (**20a**), *meta* (**20b**) and *para* (**20c**) positions.

The synthesis of intermediates **23a-c** was carried out according to the protocol previously described by our group.³⁰ Following that synthetic route, indole-3-carboxylic acid (**24**) was treated with oxalyl chloride and DMF to obtain the

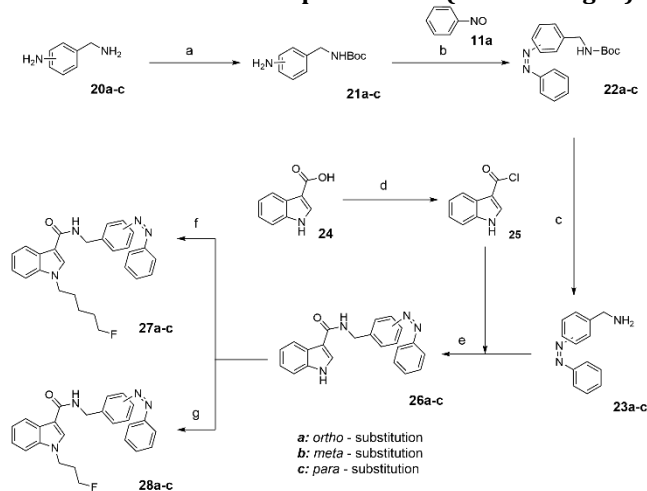
corresponding acyl chloride **25**. Coupling between intermediate **25** and amines **23a-c** resulted in the formation of the amides **26a-c**. Subsequently, deprotonation with NaH and addition of 1-bromo-pentane or 3-fluoropropyl 4-methylbenzenesulfonate yielded compounds **27a-c** and **28a-c** with a fluorinated chain of 5 and 3 carbon atoms, respectively.

Scheme 2. Synthesis of photo-CB₁R ligands with introduction of azobenzene in position C-3 (ketone bridged).^a



^aReagents and conditions: (a) MeMgBr, THF, -78°C, 4h; (b) LiOH, MeOH, THF, rt, 2h, 10-53%; (c) 1-bromo-5-fluoropentane, NaH, DMF, 65°C, 3h, 74-81%; (d) H₂, Pd/C, EtOH, rt, 2h, quant; (e) AcOH/TFA/toluene, rt, overnight, 14-22%.

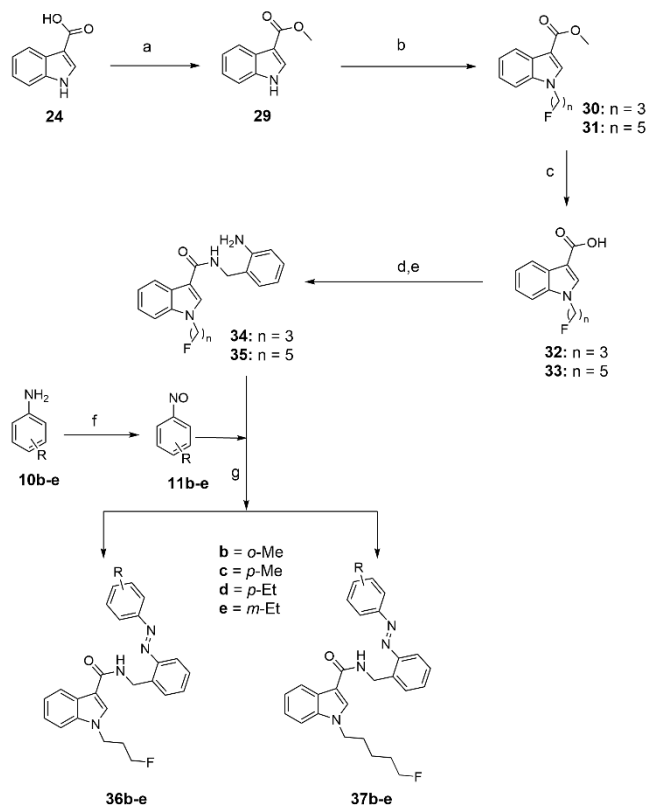
Scheme 3. Synthesis of photo-CB₁R ligands with introduction of azobenzene in position C-3 (amide bridged).^a



^aReagents and conditions: (a) TEA, Boc₂O, DCM, 0°C, 2 h, quant; (b) nitrosobenzene, acetic acid, rt, overnight, 58-68%; (c) TFA, DCM, rt, overnight, quant; (d) (COCl)₂, DMF, DCM, 0°C→rt, 2 h; (e) TEA, DCM, 0°C→rt, 30 min, 50%; (f) 1-bromo-5-fluoropentane, NaH, DMF, 65°C, 3h, 32-48%; (g) 3-fluoropropyl 4-methylbenzenesulfonate, NaH, DMF, 65°C, 3h, 19-29%.

Considering the ease in the synthesis of amide bridged photo-ligands (compared to the low yields obtained in the coupling with ketone bridges), and in view of the highly hydrophobic nature of CB₁R, the following synthesis was planned by introducing small aliphatic substituents in the distal ring of azobenzene to analyze whether these changes translate into a greater difference between the *cis* and *trans* isomers. The new molecules are derivatives of the target compounds **27a** and **28a**, whose modifications allowed us to evaluate the effect of azobenzene substitution regarding the affinity for CB₁R (Scheme 4).

Scheme 4. Derivatization of *ortho*-substituted amide bridged photo-CB₁R ligands.^a



^aReagents and conditions: (a) MeOH, H₂SO₄, 80°C, 94%; (b) Alkyl fluoride, NaH, DMF, 65°C, 3h, 92-98%; (c) NaOH, EtOH, 80°C, 2 h, 86-98%; (d) (COCl)₂, DMF, DCM, 0°C→rt, 2 h; (e) 2-aminobenzylamine, TEA, DCM, 0°C→rt, 30 min, 97%; (f) MPS, DCM/H₂O, rt, overnight; (g) AcOH, rt, overnight, 11-71%.

As in the previous synthetic route, the synthesis began with compound **24**, whose carboxylic acid esterified by a reaction with MeOH and H₂SO₄, generating the ester **25**. The indole was deprotonated at position *N*-1 with sodium hydride and subsequently by reaction with alkyl fluoride, yielding intermediates **30** and **31** with 3 and 5 carbon atoms in the side chain respectively. Subsequently, basic hydrolysis of the ester was carried out, generating intermediates **32** and **33**. The carboxylic acid was activated with oxalyl chloride, and subsequently added to a solution of 2-aminobenzylamine and TEA to yield the *ortho*-substituted anilines **34** and **35**. In parallel, the nitroso compounds **11a-e** were obtained *in situ* from the partial oxidation of the anilines **10a-e** with

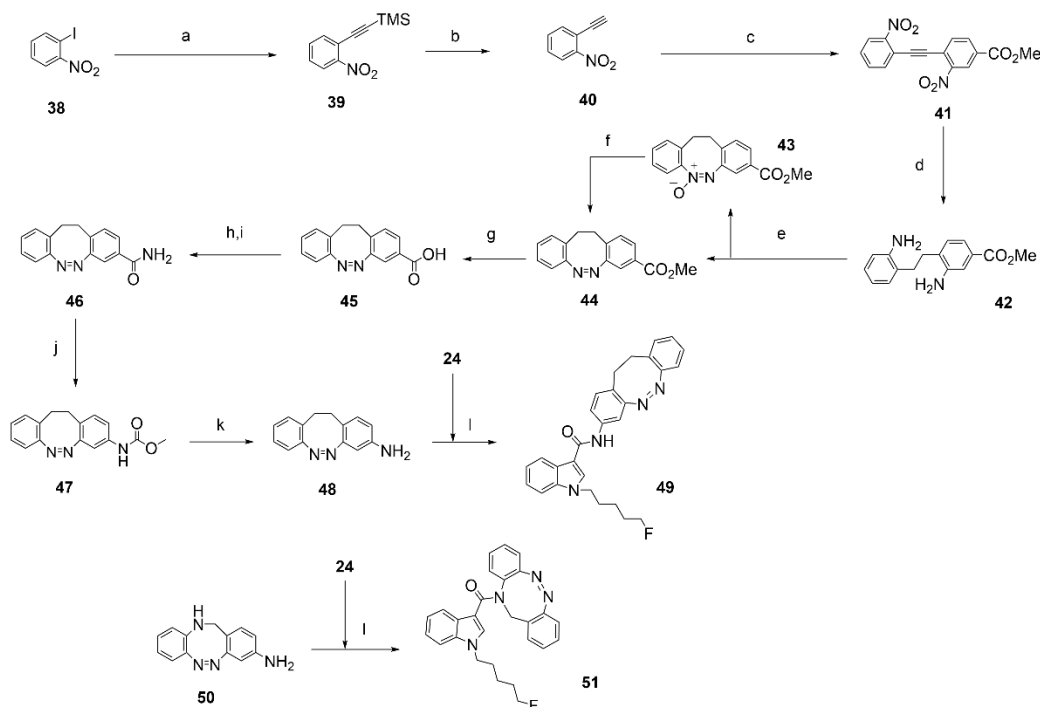
MPS. The coupling between nitroso compounds **11a-e** and anilines **34** and **35** was carried out with the Baeyer-Mills reaction under acid conditions to generate the final compounds **36a-e** and **37b-e**, respectively with 3 and 5 carbon atoms in their side chain.

Classical azobenzenes are thermodynamically stable in their *trans* isomer, undergoing isomerization to their *cis* form by light irradiation with wavelengths in the UV region of the spectra, and relaxation to their stable photoisomers by irradiation with wavelengths $\lambda > 400$ nm.³⁸ However, recent publications have detailed the characterization of cyclic azobenzenes, which - and in contrast to classical azobenzenes - are thermodynamically stable in their *Z* form. These diazocines are isomerized to their *E* isoform by irradiation $\lambda < 400$ nm and converted back to their *Z* isomer by irradiation at wavelengths $\lambda > 500$ nm.³⁹⁻⁴¹ Given that only few publications to date have explored these novel azobenzenes for pharmacological applications,^{42, 43} we carried out a synthetic route for incorporation of diazocines into the central ring of the indole through amide bridge formation (Scheme 5).

The synthetic route started with a Sonogashira coupling reaction between aryl-iodide **38** and TMS-acetylene, yielding compound **39**. Subsequent elimination of TMS with K_2CO_3 in MeOH generated intermediate **40**, which reacted in a second Sonogashira coupling reaction with methyl 4-iodo-3-ni-

trobenzoate to give rise to molecule **41**. Simultaneous reduction of the alkyne and the two nitro groups by hydrogenation at high pressure yielded diamine **42**. Subsequently, slow addition of a *m*CPBA solution to compound **42** allowed partial oxidation of one of the anilines to nitroso, which reacted intramolecularly to yield diazocine **44**. However, the byproduct azoxyazobenzene **43** was also formed. To increase the overall yield, we adapted a procedure of the literature,⁴⁴ treating byproduct **43** with $MoO_2Cl_2(dmf)_2$ and PPh_3 to deoxygenate to the corresponding azobenzene **44**. Carboxylic acid **45** was obtained by hydrolysis of **44** under basic conditions with NaOH and EtOH. The carboxylic acid was then activated with oxalyl chloride and further reacted with aqueous ammonia solution to give the primary amide **46**. Subsequently, a Hofmann rearrangement with metallic sodium and NBS generated carbamate **47**. Hydrolysis of the carbamate to the corresponding primary amine **48** was achieved by hydrolysis under basic conditions with NaOH. Finally, coupling of the amine **48** and the carboxylic acid **24** was achieved by Mukaiyama reagent and DIPEA, giving the target *C*-diazocine **49**. In parallel, the azobenzene **50** was synthesized according to the protocol previously described in literature.⁴¹ This last intermediate **50** reacted with Mukaiyama reagent and DIPEA, yielding the target *N*-diazocine **51**.

Scheme 5. Synthesis of photo-CB1R ligands as C-3-indole-coupled diazocines. ^a



^aReagents and conditions: (a) CuI , $PdCl_2(PPh_3)_2$, TMS-acetylene, TEA, THF, rt, overnight, quant; (b) K_2CO_3 , MeOH, rt, 10 min, 75%; (c) methyl 4-iodo-3-nitrobenzoate, CuI , $PdCl_2(PPh_3)_2$, TMS-acetylene, TEA, THF, rt, 72 h, 72%; (d) H_2 , Pd/C, MeOH, rt, 5 h, 10 bar, 97%; (e) *m*CPBA, AcOH, DCM, rt, slow addition over 12 h, 52-70%; (f) PPh_3 , $MoO_2Cl_2(dmf)_2$, THF, 70°C, 3 h; (g) NaOH, EtOH, 80°C, 2 h, 76%; (h) $(COCl)_2$, DMF, DCM, 0°C, 1 h; (i) DCM, NH_4OH , 0°C→rt, 30 min, 63%; (j) Na, NBS, MeOH, 65°C, 1.5 h, 64%; (k) NaOH, MeOH, 70°C, 12 h, quant; (l) 2-chloro-1-methylpyridinium iodide, DIPEA, DCM, rt, 4 h, 41-52%.

Photophysical properties. All the target compounds were photocharacterized by UV/vis spectroscopy. The isomeri-

zation capacity was tested by applying external light irradiation at different wavelengths to find the most suitable ones for achieving maximal conversion to their respective photo-

isomeric forms. It was found for all target compounds that the maximum photoconversion by light radiation was reached in a short period of time ($t < 2$ min). Target compounds with classical azobenzenes showed the highest photoconversion to their *cis* photo-form with UV light ($\lambda = 366$ nm) and isomerized back to their thermodynamically stable *trans* photoisomer with blue light ($\lambda = 400$ -450 nm) (**Figure 1a**). This photoconversion of classical azobenzenes is given by the $\pi \rightarrow \pi^*$ and $n \rightarrow \pi^*$ energy transitions, typical for this class of molecules.⁴⁵ As we expected, the absorption bands due to the $\pi \rightarrow \pi^*$ excitation of diazocines **49** and **51** were redshifted, being isomerized to their thermodynamically less stable isomer *E* with light irradiation at $\lambda = 400$ nm, and a photoisomerization back to the stable *Z*-photoform at high wavelengths ($\lambda \geq 530$ nm) (**Figure 2a**).

To evaluate a possible loss of photochromic behavior (photofatigue) after multiple cycles of *trans*→*cis*→*trans* isomerization, the target compounds were evaluated at the wavelength of maximum absorption for each case. The classical azobenzenes samples were prepared in a 50 μ M DMSO solution for UV/Vis characterization, while the diazocines, due to their very low absorption, had to be prepared in higher concentrations (200 μ M). The compound solutions were consecutively irradiated with wavelengths at which the maximum photoconversion was obtained for its two photoisomers ($\lambda = 366$ nm for *cis* and $\lambda = 400 - 450$ nm for *trans*). After 10 cycles, all target compounds were shown to be stable without significant changes in the absorption values (**Figure 1b**). Target compounds **49** and **51** did not show photofatigue either (**Figure 2b**), however, unlike the classic azobenzenes, both diazocines show a change in hue when they are photoconverted. In this way, in its thermodynamically stable isomer (*Z*), a methanolic solution of the final compound showed a pale-yellow color, however, when irradiated with UV light $\lambda = 400$ nm, the target compounds presented a pink or violet coloration in their *E*-photo-isomer. Additionally, when exposed to ambient light, or irradiated again with amber-red light, the diazocines switched back to their initial color. This process could be repeated for several cycles with no apparent loss of hue (**Figure 2c**).

As photoswitching and thermal relaxation is solvent dependent, we also evaluated the azobenzene based compounds in aqueous environment. Most of the compounds showed long thermal stability when a 50 μ M (DMSO:buffer (4:1), pH = 7.4) solution photoisomerized to their thermodynamically less stable photo-form and stored into the dark (3h, 37°C) (**Figure 1c** and Supporting Information, **Table S3**), without significant photoconversion under the assay conditions. Additionally, the photostationary distribution of the compounds was quantified by HPLC. The analyses were performed at the isosbestic point of the UV spectrum for each substance, by testing a methanolic solution of the respective target compound. The final compounds containing a classical azoben-

zene moiety were distributed mainly towards their thermodynamically stable *trans* (70 - 85%) isomer. When measured after irradiation with UV light ($\lambda = 366$ nm), the ratio of *cis* isomer increased considerably, becoming the predominant photo-form. Meanwhile, diazocines **49** and **51** were distributed almost entirely to their thermodynamically stable isomer *Z* (>90%). When measured after irradiation with light $\lambda = 400$ nm, the proportion of *E*-photo-isomer increased, however, in contrast to classical azobenzenes, it was only possible to obtain a mixture 1:1 of both photo-forms (c.f. **Supporting Information, Figures S22a-b and S23a-b**).

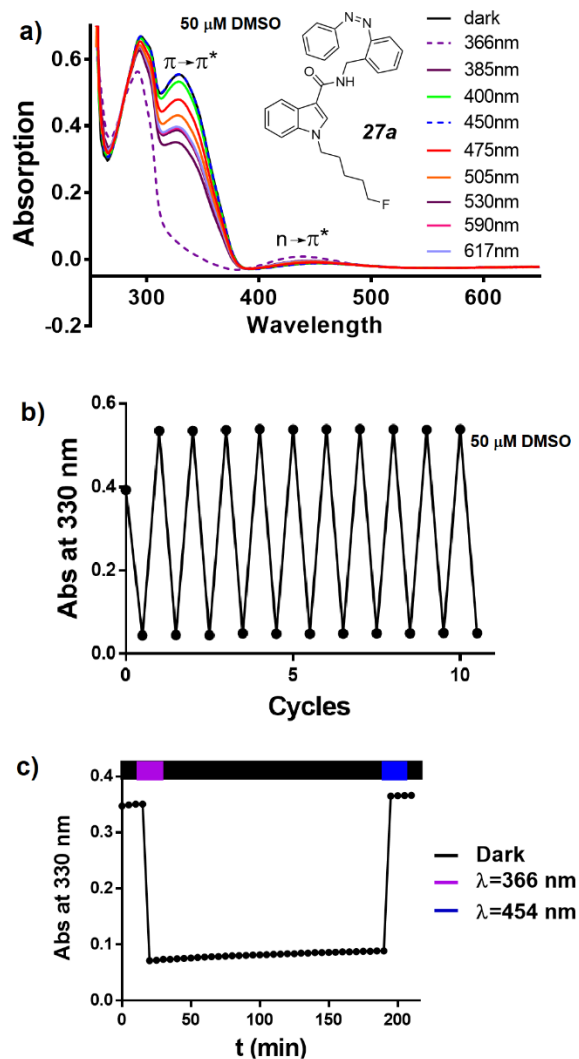


Figure 1. Photochemical characterization of classic azobenzene **27a**. **a)** Changes in the absorption spectrum upon irradiation with different wavelengths. **b)** Absence of photofatigue after 10 switching cycles. **c)** Thermal stability in a period of 3 h at 37 °C, 50 μ M (DMSO : buffer pH 7.4 (4:1)).

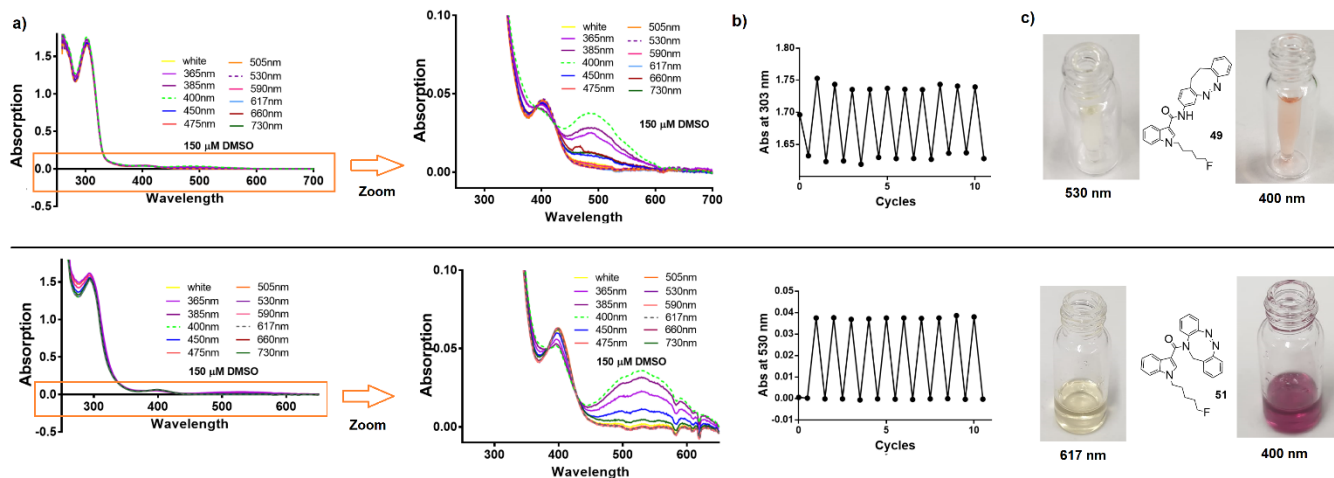


Figure 2. Photochemical characterization of diazocines **49** (up) and **51** (down). **a**) Changes in the absorption spectrum upon irradiation with different wavelengths (Full Spectrum and Y-Axis Zoom). **b**) Absence of photofatigue after 10 switching cycles. **c**) Notorious color changes shown in their photostates (4 mM methanolic solution).

Radioligand binding studies. After carrying out the photocharacterization of the target compounds, their affinity for CBRs was evaluated in radioligand binding assays. This assay was chosen as the first filter, because unlike optical assays *in vitro*, it can be performed without the need for any external light sources.^{30, 46, 47} This makes it easy to exclude possible false negatives due to back-isomerization of the ligands during the assay run or reading process. The radioligand binding studies are useful to check to which extent structural differences between each pair of photo-isomers translate into changes in the affinity to the receptor. A photoswitchable ligand with a marked difference in affinity can be switched from a low-activity state "switch-off" to a high-activity state "switch-on" or *vice versa*, by external light irradiation.

In the competition assays, most of the final compounds showed affinity for CB₁R in the 1-digit micromolar range (**Table 1**). Compounds with azobenzene attached to the indole by position *N*-1 showed low affinity for CB₁R. Specifically, compound **12b** was unable to displace the reference CP55940 in the assays for both CB₁R and CB₂R. Similarly, compounds with a 3-carbon side chain attached to nitrogen showed a lower affinity for CBRs compared to their 5-carbon chain counterparts. This goes along with the keto bridged compounds (3C-chain) **28b** and **28c**, who did not displace the radioligand in the assay. Additionally, when comparing the compounds of the **36b-e** family with their **37b-e** homologues, the compounds with a short side chain had lower affinity for the receptor, even without showing any binding in some cases (**36c-trans**, **36e-cis**). This indicates that although short-chain agonist compounds with high affinity are found in the literature,^{14, 31} nevertheless, for the compounds described in this project, the presence of a chain of at least 5 carbon atoms is preferable.

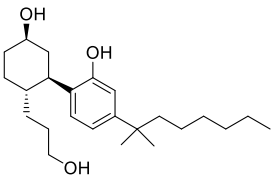
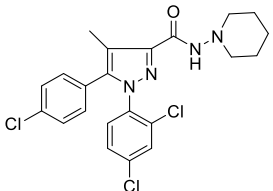
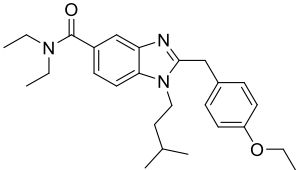
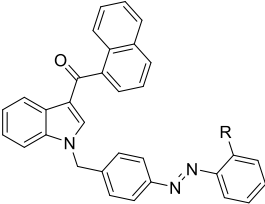
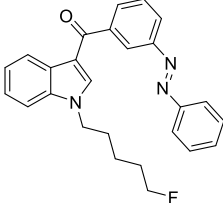
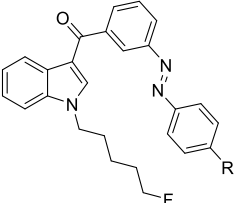
The best example of the above findings is observable when comparing analogs **27a** (5 carbon atoms in the side chain) and **28a** (3 carbon atoms in the side chain). Regarding the

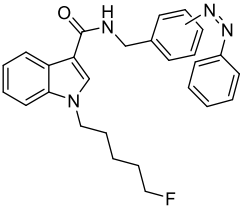
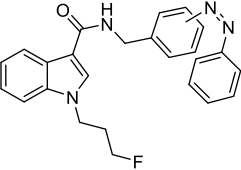
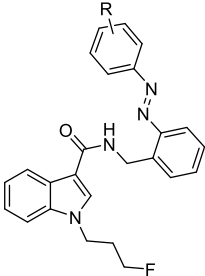
effect of aromatic substitution of the azobenzene-photoswitch, both *ortho*-substituted compounds showed higher affinity values for CB₁R compared to the respective *meta* (**27b**, **28b**) and *para* (**27c**, **28c**) substituted analogues. This could be explained based on data from the literature, where CB₁R indole-based agonists with unsubstituted benzylic position had lower potency and affinity for CB₁R compared to analogues with methyl or cumyl substitution.³³ For this project, the distal azobenzene ring of the target **27a** and **28a** *ortho*-photocompounds could occupy a cavity in the vicinity of the carbonyl group when the compounds are in the *cis* form. However, *meta*- and *para*-analogs fall short of occupying this position upon isomerization. This theory is reinforced by analyzing the *trans* photoforms of **27a** and **28a**, which could not occupy this hydrophobic region necessary for activity, so they have a lower affinity for CB₁R compared to their **27a-cis** and **28a-cis** counterparts, respectively.

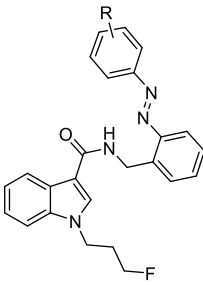
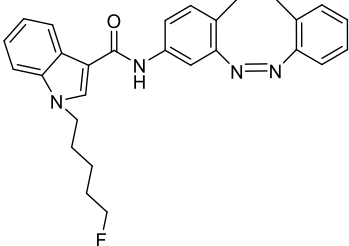
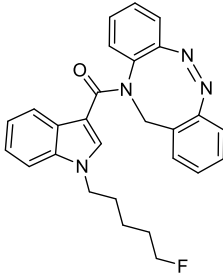
Similarly, both compounds **27a** and **28a** show higher affinity when compared to their derivatives with distally substituted azobenzene (**37b-e** and **36b-e**, respectively), suggesting that the unsubstituted azobenzene ring might have less steric hindrance when binding to CB₁R. Despite these similarities between both analogs, compound **27a** showed superior binding affinities for CB₁R in the sub-micromolar range (CB₁R Ki **27a-cis** = 0.18 μM; CB₁R Ki **27a-trans** = 0.97 μM) and the largest difference between both photo-isomers (*trans/cis* ratio = 5.4-fold) (**Figure 3a**), which reaffirms the importance of a long side chain for this type of substances. Additionally, when performing binding studies in CB₂R, we found that photo-isomer **27a-cis** has a 6.8-fold higher selectivity for CB₁R compared to CB₂R (CB₂R Ki **27a-cis** = 1.22 μM).

When comparing the classic azobenzenes with the diazocines, it was found that this last class of compounds presents a moderate affinity in both isomers in the binding studies and fairly low differences between the photo-isomers. But in fact, the *Z*-photo-isomer, which is more stable in this case, was also the photo-form with the higher affinity, which demonstrates the feasibility of this approach.

Table 1. Affinity values at *rCB₁R* and *hCB₂R* determined in radioligand binding studies.

	Photoisomers	<i>rCB₁R</i> pK _i ± SEM ^a	CB ₁ trans / cis ratio	<i>hCB₂R</i> [³ H] CP55950 displ. at 1 μM or <i>hCB₂R</i> pK _i ± SEM ^b	
CP55940		9.54 nM (8.02 ± 0.054)	-	13.7 nM (7.86 ± 0.071)	
Rimonabant		62.9 nM (7.20 ± 0.07)	-	< 10%	
Reference compound 52*		-	-	64.8 nM (7.19 ± 0.04)	
12					
12a	R = H	cis	2.38 μM (5.62 ± 0.12)	3.8	29%
		trans	9.17 μM (5.04 ± 0.43)		35%
12b	R = CH ₃	cis	<10%	-	12%
		trans	<10%		23%
18					
		cis	2.34 μM (5.63 ± 0.09)	0.9	73%
		trans	2.12 μM (5.67 ± 0.17)		76%
19					
19a	R = H	cis	2.12 μM (5.67 ± 0.13)	1.6	64%
		trans	3.32 μM (4.58 ± 0.17)		64%
19c	R = CH ₃	cis	3.98 μM (5.40 ± 0.18)	0.7	44%

		trans	2.87 μM (5.54 \pm 0.41)		43%
27					
27a	<i>ortho</i> -substitution	cis	0.18 μM (6.75 \pm 0.07)	5.4	1.22 μM (5.99 \pm 0.08)
		trans	0.97 μM (6.01 \pm 0.08)		3.55 μM (5.45 \pm 0.07)
27b	<i>meta</i> -substitution	cis	3.07 μM (5.51 \pm 0.10)	0.4	31%
		trans	1.15 μM (5.94 \pm 0.28)		25%
27c	<i>para</i> -substitution	cis	3.73 μM (5.43 \pm 0.12)	0.5	25%
		trans	1.85 μM (5.73 \pm 0.17)		30%
28					
28a	<i>ortho</i> -substitution	cis	1.28 μM (5.89 \pm 0.20)	3.3	35%
		trans	4.29 μM (5.37 \pm 0.25)		39%
28b	<i>meta</i> -substitution	cis	<10%	-	19%
		trans	<10%		14%
28c	<i>para</i> -substitution	cis	8.49 μM (5.07 \pm 0.49)	-	19%
		trans	<10%		22%
36					
36b	R = <i>o</i> -Me	cis	4.97 μM (5.30 \pm 0.25)	0.7	14%
		trans	3.58 μM (5.45 \pm 0.41)		25%
36c	R = <i>p</i> -Me	cis	11.20 μM (5.37 \pm 0.25)	-	24%
		trans	<10%		21%
36d	R = <i>p</i> -Et	cis	7.34 μM (5.13 \pm 0.73)	2.0	16%
		trans	15.13 μM (4.82 \pm 0.42)		24%
36e	R = <i>m</i> -Et	cis	<10%	-	22%
		trans	6.05 μM (5.21 \pm 0.51)		17%

37						
	37b	R = <i>o</i> -Me	<i>cis</i>	2.27 μ M (5.64 \pm 0.18)	1.1	42%
			<i>trans</i>	2.55 μ M (5.59 \pm 0.14)		34%
37c	R = <i>p</i> -Me	<i>cis</i>	1.08 μ M (5.96 \pm 0.12)	1.3	34%	
		<i>trans</i>	1.36 μ M (5.86 \pm 0.09)		18%	
37d	R = <i>p</i> -Et	<i>cis</i>	0.56 μ M (6.25 \pm 0.11)	2.2	90%	
		<i>trans</i>	1.25 μ M (5.90 \pm 0.17)		70%	
37e	R = <i>m</i> -Et	<i>cis</i>	0.88 μ M (6.06 \pm 0.10)	1.7	65%	
		<i>trans</i>	1.49 μ M (5.83 \pm 0.13)		41%	
49						
			Z	4.72 μ M (5.33 \pm 0.18)	0.3	18%
			E	1.57 μ M (5.80 \pm 0.09)		18%
51						
			Z	7.31 μ M (5.14 \pm 0.41)	0.7	32%
			E	5.23 μ M (5.28 \pm 0.15)		38%

^a Performed on CB₁ membranes prepared from rat brain homogenate.

^b Performed on CB₂ membranes harvested from stably transfected hCB₂-HEK-293 cells.

* Internal reference compound used for CB₂ binding experiments.⁴⁸

Cannabinoid receptor internalization. We next sought to determine efficacy using internalization of the receptors as a readout. The best compounds - according to the results of our radioligand binding assay - were evaluated regarding their effect on endocytosis of FLAG-epitope-tagged CB₁ and CB₂ receptors stably expressed in HEK293 cells, detected by fluorescently conjugated M1-anti-Flag antibody,⁴⁹ and mon-

itored by flow cytometry. Compounds were tested as agonists, expressed as percentage of internalization caused by CP55940, and as antagonists against 10 nM CP55940, in both the *cis* and *trans* forms. Irradiation with the respective wavelength was done for the dilution rows in DMSO before addition to the wells. Compound **27a** behaved as an agonist for both photo-isomeric forms, with the *cis*-isomer showing 4.4-fold elevated potency and efficacy (PSS_{365nm}, EC₅₀ (CB₁))

= 154 nm) (**Figure 3b**). This pronounced agonist profile of the *cis* isomer is consistent with the results previously obtained by radioligand binding assay. When analog **27a** was tested, the compound did not show agonist or antagonist behavior in endocytosis at the CB₁R, whereas the parent compound **4** (EC₅₀ (CB₁) = 5.4 nM) proved to be an equally good agonist as CP55940 (EC₅₀ (CB₁) = 1.1 nM). Compound **27a** was also tested against CB₂R to study selectivity. At 10 μM the amount of internalized CB₂ receptor was 53 % of the maximum response caused by CP55940 (data not shown), proving that the compound acts as selective CB₁R agonist in the relevant concentration range.

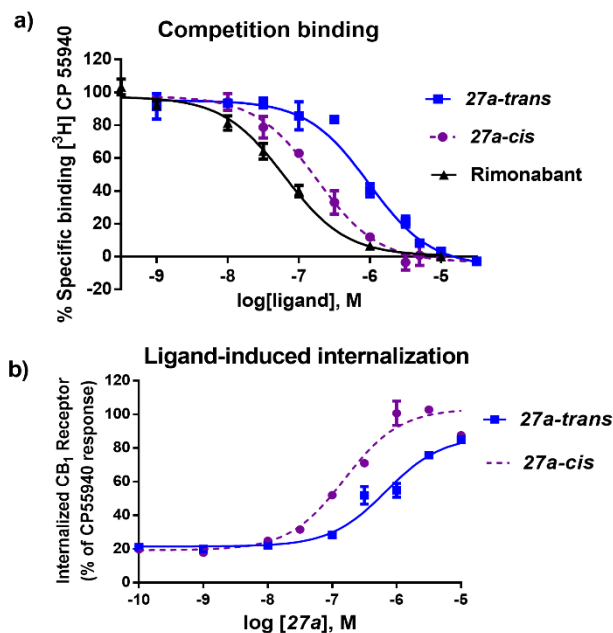


Figure 3. Pharmacological evaluation of compound **27a**. **a)** Radioligand binding assay: *cis* (purple, dotted line) and *trans* (blue, solid line) photo-isomers vs. rimonabant as control. Each data point and error bar represent the average of 3 independent experiments by triplicate ± standard error of the mean (SEM). **b)** Ligand-induced internalization in HEK293 cells. Data of compound **27a**. Each data point and error bar represent the average of 3 independent experiments ± standard error of the mean (SEM).

GRABeCB_{2.0} sensor assay. To test the biological activity of the most active compound at the receptor level, we decided to directly measure the activity at CB₁R, using a genetically encoded fluorescent CB₁R sensor named GRABeCB_{2.0}.⁵⁰ For the biosensor design, a circularly-permuted green fluorescent protein (cpGFP) was inserted into a conformationally sensitive domain between transmembrane domains 5 and 6 of CB₁R. When testing an agonist substance capable of binding to the sensor protein, a strong increase in sensor fluorescence is generated, indicating receptor activation. For this project, an assay was designed in a 96-well plate using HEK293T cells with transient expression of GRABeCB_{2.0}. Subsequently, the reference CB₁R agonist CP55940 was

tested (**Figure 4a**), showing a concentration-dependent increase in fluorescence (EC₅₀: 64.8 nM), thus indicating the activation of GRABeCB_{2.0}.

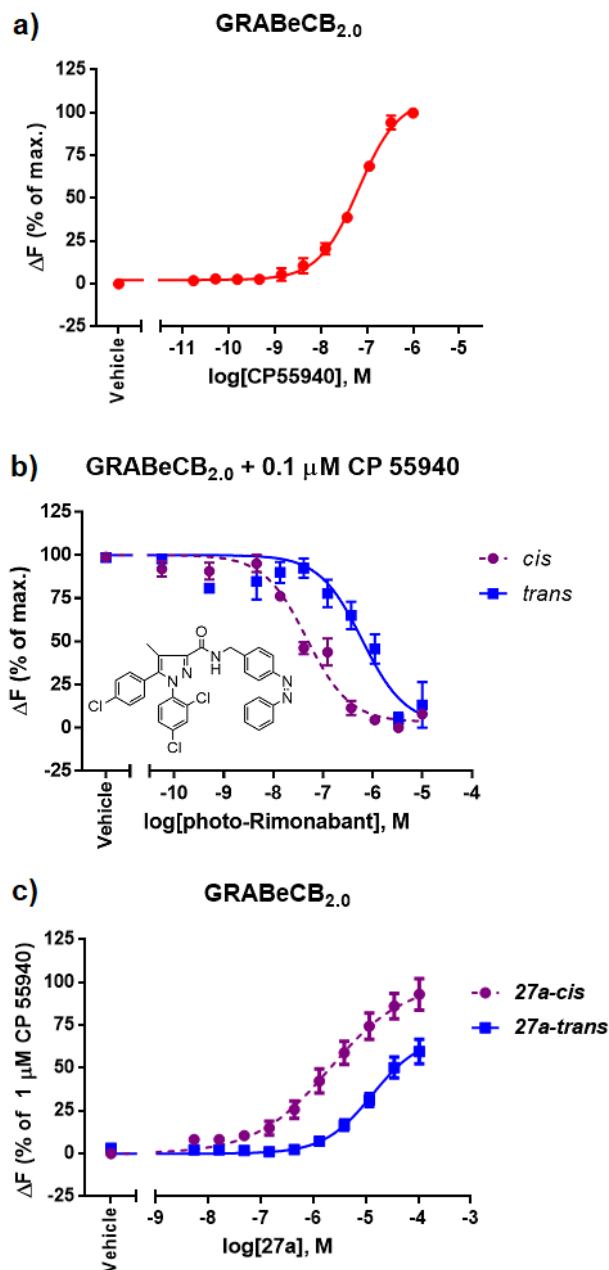


Figure 4. CB₁R-cpGFP sensor assay. **a)** Dose-dependent activation of GRABeCB_{2.0} by CP55940. **b)** Dose-dependent inhibition of 0.1 μM CP55940-induced GRABeCB_{2.0} response by photo-rimonabant: Fluorescence was measured at each well before and after addition of different concentrations of *cis* (purple, dotted line) or *trans* (blue, solid line) photo-rimonabant to calculate ΔF. **c)** Dose-dependent activation of GRABeCB_{2.0} by compound **27a**: Fluorescence was measured at each well before and after addition of different concentrations of *cis*- or *trans*-**27a** to calculate ΔF. For all the curves each data point and error bar represent the average of 3 independent experiments (7 independent experiments for **4c**) ± standard error of the mean (SEM).

Once the assay was validated with the reference agonist ligand, we wanted to assess whether the GRABeCB2.0 assay is feasible to study photoswitchable CB₁R ligands. To do so, we tested the previously described antagonist "photo-rimonabant" in this assay.³⁰ Our group previously reported that photo-rimonabant is more active in its *cis* photo-form. For this assay, we observed that *cis*-photo-rimonabant inhibits the CP55940-mediated activation of GRABeCB2.0 with a concentration-dependent fashion. The *cis*-photo-isomer inhibited GRABeCB2.0 response with 13-fold higher potency than *trans*-photo-rimonabant did (**Figure 4b**), exhibiting IC₅₀ values in agreement with our last publication (IC₅₀*cis*: 47 nM, IC₅₀*trans*: 613 nM).³⁰ With these data, we were able to verify the suitability of the GRABeCB2.0 assay for studying the pharmacology of photo-switchable CB₁R ligands.

Next, we studied the activity of **27a** photo-isomers using the GRABeCB2.0 assay. In these experiments, both *cis*- and *trans*- photo-forms of **27a** displayed a concentration-dependent activation of GRABeCB2.0, confirming their agonistic characters. The isomer **27a-cis** displayed a higher maximal response (93% of response induced by 1 μM CP55940) than **27a-trans** (59.6%). Moreover, in its *cis* isomer, ligand **27a** activated GRABeCB2.0 6-fold more potently than its *trans* isomer (EC₅₀*cis*: 2.1 μM, EC₅₀*trans*: 13.3 μM) (**Figure 4c**). The observed fold difference in EC₅₀ was in accordance with the ones observed in the binding studies and internalization of the target compound. To validate the ligand-specific activation of the eCB2.0 sensor, we performed a negative control experiment in which we tested **27a** on cells expressing an inactive mutant of the eCB2.0 sensor. In these experiments, neither the CB₁R agonist CP55940 nor the *cis* or *trans* isomers of **27a** activated the sensor. These results indicate that the activation of eCB2.0 sensor by **27a** is a ligand specific response, and not an artefact (data not shown).

51

hCB₁R calcium mobilization assay. To further characterize the target compounds, an intracellular fluorescent hCB₁-activated G_{αq16}-coupled calcium mobilization assay was performed. This assay used CHO-K₁ cells overexpressing hCB₁R as has been described in previous studies.^{30, 52} The compounds were tested as both photo-isomers. For the photo-isomerization, a DMSO/buffer dilution (< 1 % DMSO) was irradiated with the respective wavelength prior to the experiment. CP55940 was used as CB₁R agonist reference. Although this technique in our laboratory has lower sensitivity for substances with affinity in the micromolar range, it was possible to evaluate compound **27a** which was found to exert the desired agonism for hCB₁. Although the determined half maximal effective concentration was lower than for the reference substance (CP55940, IC₅₀ = 14.8 nM; **27a-cis**, IC₅₀ = 3.10 μM), it was confirmed that the photoswitchable compound has a higher efficacy in its *cis*-activated form (**Figure 5**). In its *trans* photo-isomer, compound **27a** did only present an apparent effect at even higher concentrations. This can be explained by previous data from our radioligand binding assay, giving its affinity is in the micromolar range. All other synthesized compounds failed to show similar efficacies in calcium mobilization (data not shown).

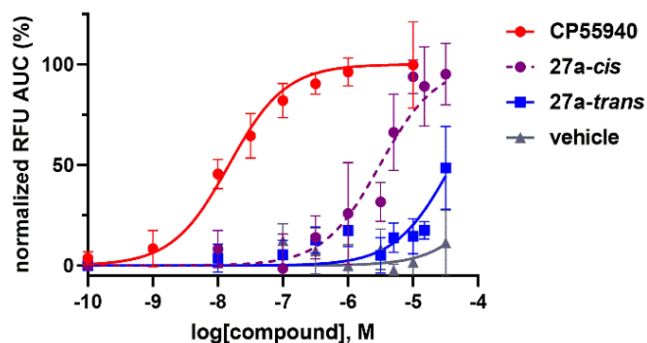


Figure 5. Calcium mobilization assay comparing the agonist CP55940 with the target compound **27a** in both photo-isomers. A higher efficacy is observed in the activated "cis-on" form compared to the less active "trans-off" isomer. Each data point and error bar represent the average of at least three independent experiments by duplicate ± standard error of the mean (SEM).

Analysis of ERK1/2 activation. CB₁R activate the extracellular signal-regulated kinases 1 and 2 (ERK1/2), that are important for cell proliferation, differentiation, and survival.^{53, 54} To evaluate the impact of the reference compound CP55940 and target compound **27a** both in the *cis* and *trans* photoform, we performed Western blot analyses to assess the phosphorylation status of ERK1/2 at the so-called TEY motif (pERK1/2), which refers to the catalytic activity of the kinases. After a 15 min stimulation, CP55940 induced a concentration dependent increase in ERK1/2 activation (c.f. Supporting Information, **Figures S70 and S71**). The respective ERK1/2 signal of the active **27a-cis** photoform was slightly less pronounced. In addition, we observed a concentration-dependent as well as a photoform-dependent increase of ERK1/2 activation for **27a**, i.e., the **27a-cis** photoform resulted in a significantly stronger ERK1/2 phosphorylation than **27a-trans**. Of note, 100nM of **27a-cis** were sufficient to induce a significant increase of pERK1/2 compared to mock treated cells (DMSO), whereas a ten times higher concentration was needed of the **27a-trans** photoform (**Figure 6**).

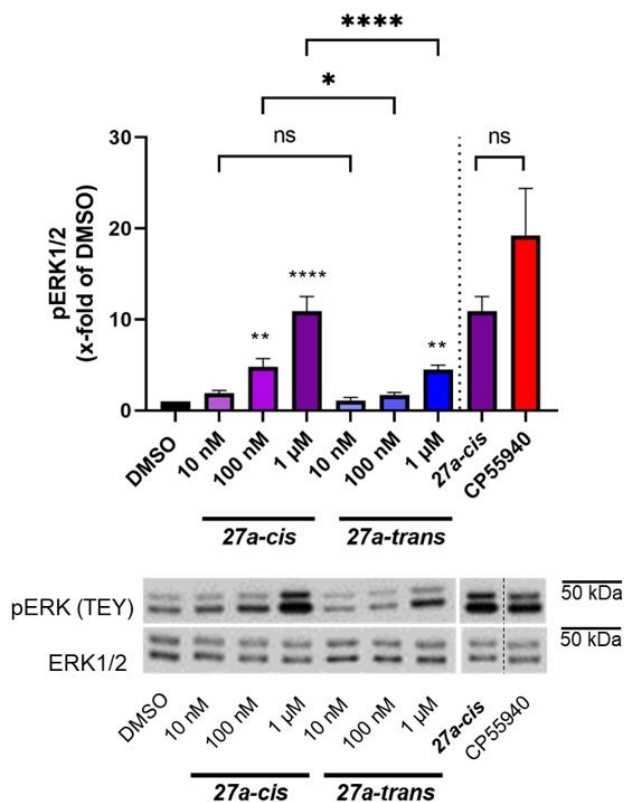


Figure 6. ERK1/2 activation by CB₁R ligands. Dose-dependent phosphorylation of ERK1/2 (pERK1/2) after CB₁R stimulation by CP55940 and **27a** both in the *cis* and *trans* photoform. The ERK1/2 phosphorylation was assessed after 15 minutes of stimulation by Western blot analyses using antibodies directed against the phosphorylated TEY motif (pERK1/2) and ERK1/2. Shown is a representative Western blot. The data represent the mean ± standard error of the mean (SEM) of 5 (*cis* and *trans* photoform of **27a**) or 6 (CP55940) experiments. For statistical analysis ordinary one-way ANOVA and Šidák's multiple comparison test as post hoc test was applied for the depicted stimulations with **27a** in the *cis* and *trans* photoform and versus DMSO, and an unpaired two-sided Student's *t*-test was applied to the 1 μM pERK1/2 signals to compare the efficacy of the target compound compared to the reference compound (1 μM **27a-cis** vs. CP55940); of note the representative blot is cut, i.e. the 1 mM band of **27a-cis** is shown twice and the uncut Western blot is shown in Supporting Information, **Figure S70**.

NanoBiT® βarr2 recruitment assays. To further assess the CB₁R activation potential of the photo-isomers of compound **27a**, a NanoBiT® luciferase assay, based on the recruitment of the intracellular signaling protein βarr2 to the ligand-activated receptor, was performed. Prior to measurements, stock solutions were irradiated with the respective wavelengths and luminescence was monitored for 2 hours. Relative to the E_{max} of the reference standard CP55,940, set at 100%, **27a-cis** was found to have an efficacy of 363%, whereas the *trans* isomer had an E_{max} of 191% compared to the reference (**Figure 7**). Furthermore, **27a-cis** had a 4-fold higher potency at CB₁ than **27a-trans** (EC_{50cis} : 221 nM, $EC_{50trans}$: 960 nM), confirming earlier findings obtained from the calcium assay, the GRABeCB2.0 sensor assay and the receptor internalization assay. At

CB₂R, both photo-isomers were found to be partial agonists compared to CP55940 with E_{max} values of 19.1% (**27a-cis**) and 26.0% (**27a-trans**) and potencies of 29.1 and 255 nM, respectively (c.f. Supporting Information, **Figure S68**).

To evaluate the reversibility of the photoswitching and the potential impact on the CB₁R activity, stock solutions containing high concentrations of **27a** were switched back and forth between *cis* and *trans* states and CB₁R receptor activation by **27a** in different phases of this cycle was measured (**Figure 8**).

In line with the previous experiments, the *cis* isomer (switched from the photostationary state to *cis*, switch 1) yielded the highest signals. Switching to *trans* (switch 2) resulted in a decrease in luminescence, which can be almost completely reversed by switching the compounds back to *cis* (switch 3), signifying that the higher activity of the *cis* isomer can be restored after earlier conversion to the *trans* isomer. After a fourth irradiation, switching **27a** to *trans*, the luminescent signal is again reduced to a similar lower level, comparable to the signal after switch 2. Overall, this shows that the different photo-isomers retain their specific activity profile after being switched back and forth between the different *cis* and *trans* states (**Figure 8**).

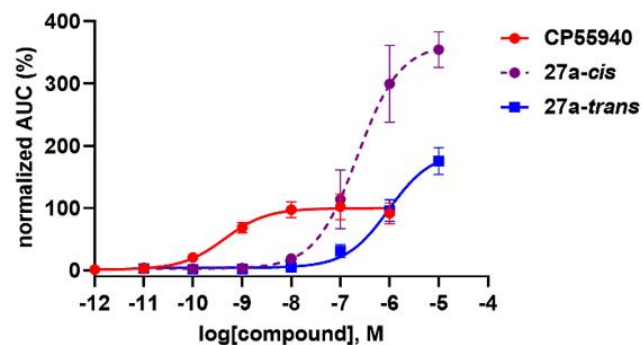


Figure 7. CB₁R βarr2 recruitment assay. Comparison of CP55940 induced βarr2 recruitment with the effect caused by compound **27a** in both photo-isomers. **27a-cis** recruits βarr2 more effectively than CP55940, but at micromolar concentrations. All data was collected from at least three independent experiments, run in duplicate.

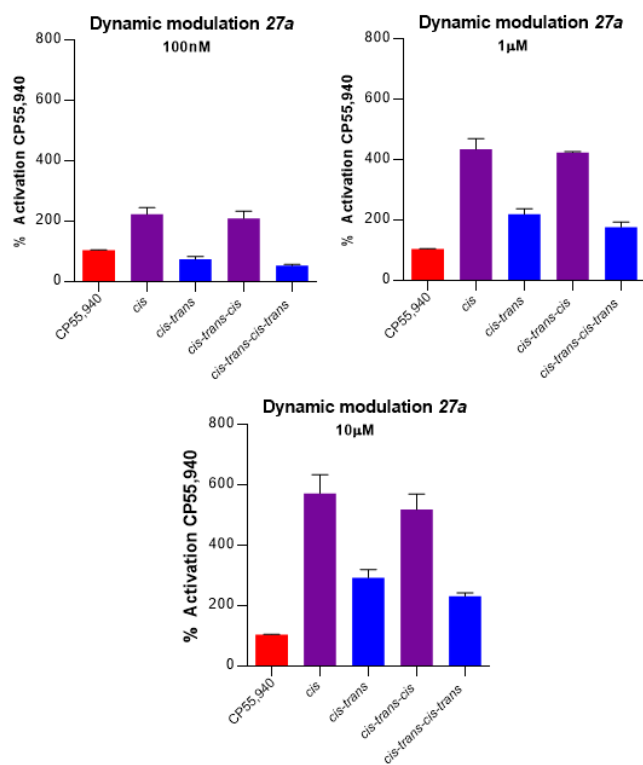


Figure 8. Dynamic photomodulation of compound **27a** at three different concentrations, demonstrated by β -arrestin2 recruitment to CB₁R. Data (n=3) is given as the mean area under the curve (AUC) \pm standard error of mean (SEM), normalized to the E_{max} of CP55940, set at 100 %.

Molecular docking. To get insights into the possible binding modes of the two photo-isomers of **27a** that could explain the differences in their binding behavior at the receptor, we used a docking routine previously optimized by us.³⁰ Briefly, the ASP⁵⁵ scoring function available within GOLD^{56, 57} was found to consistently reproduce the binding pose of the CB₁R agonist and delta-9-tetrahydrocannabinol (Δ^9 -THC) derivative, AM11542⁵⁸ (PDB ID: 5XRA), with a top-ranked pose which differed only by 0.47 Å from the experimental pose (**Figure 9a**). Docking of the AM2201³¹ derivative, reference **4**, revealed a binding mode reminiscent of AM11542. The indole core and 5-fluoropentyl tail of compound **4** occupy the same hydrophobic pocket as the 8-bromo-2-methyloctan-2-yl tail of AM11542, which is defined by F170, F189, L193, V196 and F268 (**Figures 9a and**

b). Moreover, the carbonyl group of reference **4** could form a hydrogen bond with S383, as experimentally observed for AM11542 (**Figure 9b**). Importantly, the cumyl group overlaps with the hydrophobic core of AM11542, adequately filling the pocket defined by F170, F174, F177 and F189 (**Figure 9e**). The overlapping interaction networks of compound **4** and AM11542 suggested by our docking experiments may account for the potent CB₁R agonistic effect of cumyl derivatives reported in the literature.⁵⁹ It must be noted that the docking pose of ligand **4** depicted in **Figure 9b** was ranked third best out of 50 poses, with an ASP score of 52.69. However, this pose was selected for analysis based on being in the same score range as the top ranked pose (53.84 ASP score) and its interaction network consistent with experimental data, as previously described. Additionally, rescoring with the DSX_CSD⁶⁰ scoring function yielded a better score for the selected pose than for the top ranked ASP pose (c.f. **Supporting Information, Table S1**).

Docking of the two photo-isomers of compound **27a** yielded ASP and DSX_CSD top scored poses where the indole core, carbonyl group and 5-fluoropentyl tail of the molecule occupy a similar space as in the docking result of reference **4** (**Figure 9b, c and d**). These features correspond to the common sub-structure shared by compounds **27a** and **4** and may therefore establish a similar interaction network within the orthosteric site of the CB₁R. However, our docking results suggest that the azobenzene photo-switchable group adopts a more compact conformation in the *cis* photo-isomer, occupying the same hydrophobic pocket as the cumyl group of reference **4** and the hydrophobic core of AM11542 (**Figure 9e and f**). In contrast, the distal phenyl ring of the photo-switchable group on the *trans* photo-isomer is projected beyond the experimentally observed orthosteric site of AM11542, where it may not be well packed (**Figure 9g**). We hypothesize that the more compact conformation of the *cis* photo-isomer has a better spatial arrangement in the hydrophobic cavity within the CB₁R orthosteric site. Thus, this steric arrangement may contribute to the experimentally observed 5.4-fold affinity ratio of the *cis* photo-isomer over the *trans* photo-isomer. Although the *trans* conformation has a slightly better ASP score than the *cis* conformation (68.78 vs 67.78), the scores are still within the same range as the scoring function is likely not sensitive enough to discriminate between poses with only a 5.4-fold affinity difference.

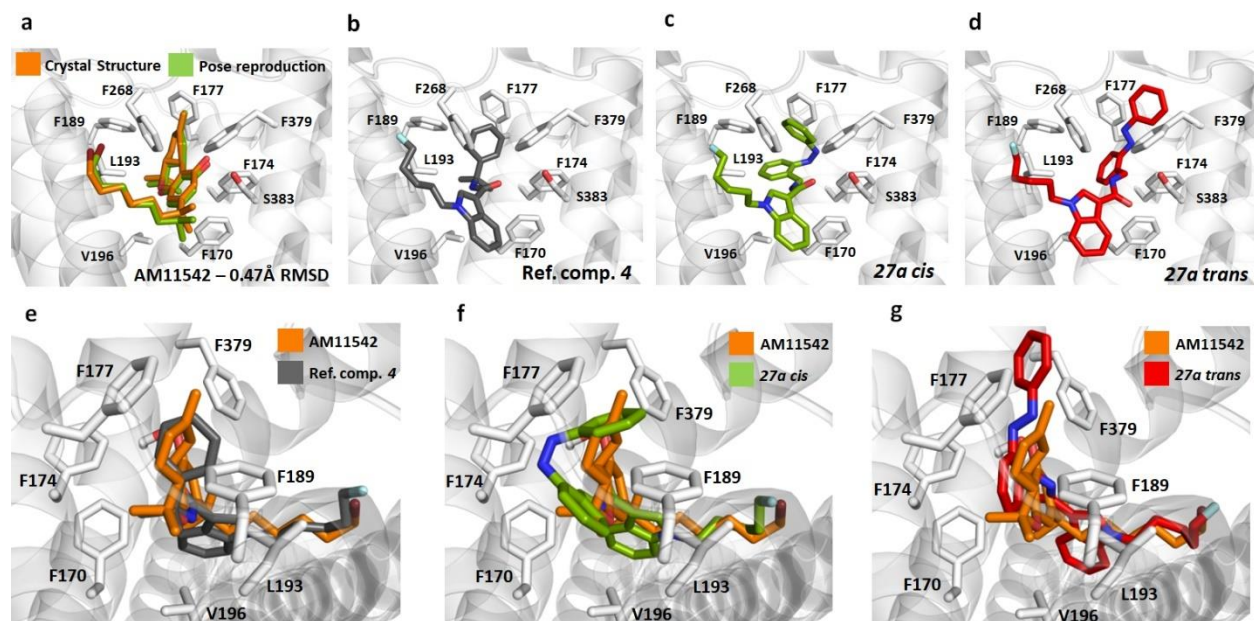


Figure 9. **a)** Pose reproduction of AM11542 (0.47Å RMSD) within the CB₁R orthosteric site. **b)** Best docking pose of reference compound **4** that resembles the binding mode of AM11542 (rank 3 of 50). **c)** Top scored docking pose of photo-isomers **27a-cis** and **d)** **27a-trans**. **e)** Experimental pose of AM11542 superimposed with the docking-predicted pose of reference compound **4** depicted in **b)**. The cumyl group occupies the same space as the hydrophobic core of AM11542. **f)** Experimental pose of AM11542 superimposed with the top scored docking pose of photo-isomer **27a-cis**, and the top scored docking pose of photo-isomer **27a-trans**. **g)** The *cis* photo-isomer assumes a more compact conformation while the *trans* photo-isomer is projected beyond the orthosteric site experimentally observed for AM11542.

A comparison of target compounds **27a** and **28a** was made to analyze the difference in affinity for CB₁R in relation to the length of the aliphatic side chain. Docking of the *cis* form of the 3-fluoropropyl derivative **28a** produced a top-scored docking pose where most structural features of the molecule (core, photoswitchable group and aliphatic chain) overlap with the top-scored docking pose of the *cis* form of the 5-fluoropentyl derivative **27a** (Figure 10a). After normalizing the ASP scores by the cubic root of the number of heavy atoms on each molecule to compensate for the bigger size of molecule **27a**, the cubic root scores (CRS)⁶¹ for the 5 best ranked poses of compound **27a** were superior to the 5 best ranked poses of compound **28a** (Supporting Information, Table S2). This is consistent with the better binding affinity experimentally observed for compound **27a** over **28a**.

Our docking results suggest that the longer aliphatic chain of target **27a** more adequately fills the side hydrophobic pocket where the tail of AM11542 is experimentally bound (Figure 10b), which may help explain the superior affinity of compound **27a** over **28a**. This observation is consistent with the experimental behavior of phytocannabinoids reported in the literature, where longer aliphatic chains such as in THCP (heptyl chain) and THC (pentyl chain), lead to a higher affinity value towards CB₁R than shorter aliphatic chains such as in THCB (butyl chain) and THCV (propyl chain).⁶²

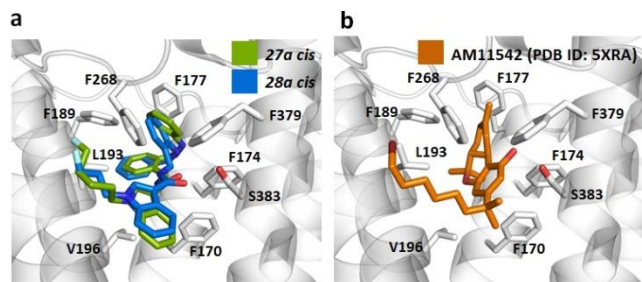


Figure 10. **a)** Top ranked docking poses of the 3-fluoropropyl (**28a**) and 5-fluoropentyl (**27a**) derivatives in their respective *cis* conformations. **b)** Experimental binding mode of AM11542.

CONCLUSIONS

By developing different synthetic pathways, we successfully synthesized 21 new target molecules as CB₁R agonists. These molecules were designed from an indole core with substitutions at *N*-1 and *C*-3 by adding an azobenzene moiety. All obtained compounds could be easily photoisomerized by external light sources. This photoconversion can be repeated for many cycles without changes in absorption spectra of the synthesized compounds. Additionally, most of the compounds show good stability of their thermodynam-

ically less stable photo-isomers after irradiation and environmental light exclusion, demonstrating good thermal stability for a period of 3 hours at 37°C.

The pharmacological characterization showed that the compounds substituted with the azobenzene moiety at *C*-3 have a higher affinity for CB₁R compared to those substituted at *N*-1. Similarly, compounds with amide bridges, aromatic substitution of azobenzene in the *ortho* position, and without additional substituents on the distal benzene ring of azobenzene are preferred. The fluorinated side chain in *N*-1 should have a length of five or more carbon atoms to enhance the potency of the compound. When evaluating all target compounds by several *in vitro* assays, it was concluded that target compound **27a**, which presents all the previously listed structural characteristics, is the one with the best pharmacological properties.

Compound **27a** shows affinity for CB₁R in the sub-micromolar range with a pronounced difference in affinity between both photo-isomers. The **27a-cis** isomer has a 5.4-fold higher affinity ($K_i(\text{CB}_1) = 0.18 \mu\text{M}$) than the **27a-trans** isomer ($K_i(\text{CB}_1) = 0.97 \mu\text{M}$). The agonistic activity of compound **27a** was verified in five different biological assays: receptor internalization, calcium mobilization, GRABeCB2.0 sensor assay, Western Blots for analysis of ERK1/2 activation, as well as in NanoBiT® β arr2 recruitment assays. In all biological assays, the pharmacological profile was similar to the one initially obtained in competition binding, showing that the **27a-cis** isomer activates CB₁R with higher potency and efficacy than the **27a-trans** photoform. This high reproducibility throughout diverse biological assays thus demonstrates the robustness of the obtained results. Additionally, we verified that compound **27a** retain its specific activity profile after several cycles of *cis-trans-cis* irradiation, allowing optical control of their pharmacological profile. This suggests that these novel compounds have a clear advantage over traditional non-switchable ligands. It should also be mentioned that the affinity difference at the receptor level seems quite low, but numerous photopharmacological tool compounds have shown much more pronounced effects in assays investigating subsequent steps in the activation cascade,^{28, 46, 47, 63} we even have recently shown an “all-or-nothing” *in vivo* response between *cis* and *trans* photoisomers.⁶⁴

The pharmacological properties mentioned above can be explained by molecular docking, whose results allow us to hypothesize that azobenzene substituted in *ortho* of the **27a-cis** isomer adopts a more compact conformation that can better fill the hydrophobic cavity at the orthosteric site of CB₁R. Meanwhile, when isomerized to the **27a-trans** photoform, the photo-switchable group is projected to a region where it is not adequately packed, resulting in a lower affinity towards CB₁R.

Our results show that agonist **27a** shows a “*cis*-on” activation, with high affinity for *h*CB₁R. These properties constitute this novel compound as a new molecular tool to obtain more profound insights in GPCR pharmacology through optical modulation of *h*CB₁R, which could allow a better understanding of the disorders associated with the endocannabinoid system in the future.

METHODS

Chemistry. General Methods. We acquired both the solvents and commonly used reagents from different commercial suppliers and they were used without further purification. Tetrahydrofuran (THF) was distilled from sodium / benzophenone under an argon atmosphere. The monitoring of the reactions was performed with thin layer chromatography (TLC) on silica gel 60 on alumina foils with fluorescent indicator, and spots were detected with UV light (254 nm). All the melting points were determined with a Stuart melting point SMP3 apparatus (Bibby Sterilin Ltd, Staffordshire, UK). Preparative TLC purification (prep-TLC) was done in house by preparing glass surface chromatographic plates (20 x 20 cm) with silica gel 60GF254 (Merck). Silica gel 60, 230–400 mesh (Merck) was used for purification by column chromatography, Nuclear magnetic resonance spectra were recorded with a Bruker AV-400 NMR instrument (Bruker, Karlsruhe, Germany) in deuterated solvents and chemical shifts were expressed in ppm (DMSO: ¹H - 2.50 ppm, ¹³C - 39.52 ppm; CDCl₃: ¹H - 7.26 ppm, ¹³C - 77.16 ppm; MeOD: ¹H - 4.87 ppm, ¹³C - 49.0 ppm; for acetone-D₆: ¹H - 2.05 ppm, ¹³C - 203.6 ppm). To monitor the purity of the products by HPLC, a Shimadzu kit, equipped with a DGU-20A3R degassing unit, a LC20AB liquid chromatograph and an SPD-20A UV / Vis detector, were used. Also, we used an LCMS 20A, mass spectra. The stationary phase was a Synergi 4 μm fusion-RP (150 x 4.6 mm) column, and a MeOH / water gradient with 0.1% formic acid was used as the mobile phase (parameters: A: water, B: MeOH, $V(\text{B})/(V(\text{A}) + V(\text{B})) = \text{from } 5 \rightarrow 90\%$ over 10 min, $V(\text{B})/(V(\text{A}) + V(\text{B})) = 90\%$ for 5 min, $V(\text{B})/(V(\text{A}) + V(\text{B})) = \text{from } 90 \rightarrow 5\%$ over 3 min). The method was performed with a flow rate of 1.0mL/min and scan range of 60-1000 m/z). All target compounds were accepted if a purity of $\geq 95\%$ was achieved. The same purity criteria was applied for testing the compounds *in vitro*. UV / Vis spectra experiments were made on a Varian Cary 50 Bio UV / Vis spectrophotometer using Hellma (Type 100-QS) cuvettes (10 mm light path).

General procedure I for Azo-Coupling under Acidic Conditions (28a, 36b-e, 37b-e). The respective amine (1 eq) and the nitroso compound (1.4 to 6 eq) were dissolved in AcOH. The mixture was stirred at room temperature overnight. After reaction, the solvent was removed *in vacuo*. The raw material was dissolved in DCM and washed with sat. aq. NaHCO₃. The organic layers were dried over Na₂SO₄, and the solvent was removed under reduced pressure. The crude was purified by flash chromatography with isocratic gradient (petroleum ether: AcOEt; 95:5→5:95) to afford the title compound.

3-(Naphthalene-1-carbonyl)-1-(4-[(1E)-2-phenyldiazene-1-yl]phenylmethyl)-1H-indole (12a). Compound **9** (30 mg, 0.08 mmol, 1 eq.) was dissolved in a mixture of AcOH/ TFA / toluene (6/ 1/ 6). To this mixture, nitrosobenzene (17 mg, 0.16mmol, 2 eq.) was added. The reaction was stirred at room temperature overnight. The mixture was diluted with ethyl acetate and washed with water. The organic layer was separated, dried over Na₂SO₄ and concentrated. The residue was purified by column chromatography (DCM/MeOH/NH₄ = 120/1/0.5) to achieve the title compound (**12a**) as an orange solid. (19%, 18 mg). m.p. 190°C. ¹H NMR (400 MHz, CDCl₃): $\delta = 8.30$ (dd, $J = 14.5, 7.9$ Hz, 1H), 8.02 (d, $J = 8.2$ Hz, 1H), 7.75 (d, $J = 8.2$ Hz, 1H), 7.72 – 7.65

(m, 4H), 7.63 (d, $J = 8.3$ Hz, 1H), 7.48 (d, $J = 6.7$ Hz, 1H), 7.33 – 7.28 (m, 3H), 7.28 (s, 2H), 7.17 (ddd, $J = 7.9, 5.4, 2.4$ Hz, 2H), 7.12 – 7.09 (m, 2H), 7.07 – 6.98 (m, 2H), 6.55 (d, $J = 8.4$ Hz, 1H), 5.07 (d, $J = 60.2$ Hz, 2H). ^{13}C NMR (101 MHz, CDCl_3): $\delta = 192.1$ (1C), 152.5 (1C), 152.4 (1C), 138.9 (1C), 138.4 (1C), 138.2 (1C), 137.2 (1C), 133.8 (1C), 131.3 (1C), 130.8 (1C), 130.2 (1C), 129.1 (2C), 128.2 (2C), 127.4 (1C), 127.2 (1C), 126.8 (1C), 126.4 (1C), 126.0 (1C), 125.9 (1C), 124.6 (1C), 124.0 (1C), 123.4 (2C), 123.2 (1C), 123.0 (1C), 122.9 (2C), 118.3 (1C), 110.4 (1C), 50.6 (1C) ppm. LC: t_{R} (min) = 10.53 (*cis*) + 11.60 (*trans*), purity = 97.4%. MS: $[\text{M}+\text{H}]^+$ calc. for $[\text{C}_{32}\text{H}_{23}\text{N}_3\text{O}]^+$ = 466.56, found 466.20. High-Resolution Mass: m/z calcd for $\text{C}_{32}\text{H}_{24}\text{N}_3\text{O}$, 466.1914; found, 466.1911.

1-(4-[(1E)-2-(2-methylphenyl)diazen-1-yl]phenylmethyl)-3-(naphthalene-1-carbonyl)indole (12b). Compound **9** (40 mg, 0.11 mmol, 1 eq.) was dissolved in a mixture of AcOH/ TFA / toluene (6/ 1/ 6). To this mixture, nitrosotoluene (78 mg, 0.64 mmol, 6 eq.) was added. The reaction was stirred at room temperature overnight. The mixture was diluted with ethyl acetate and washed with water. The organic layer was separated, dried over Na_2SO_4 and concentrated. The residue was purified by column chromatography (DCM/MeOH/ $\text{NH}_4 = 99/1/0.5$) to achieve the title compound (**12b**), as an orange solid. (26%, 13.2 mg). m.p. 167°C. ^1H NMR (400 MHz, CDCl_3): $\delta = 8.51$ (dd, $J = 13.9, 8.0$ Hz, 1H), 8.22 (dd, $J = 13.7, 8.4$ Hz, 1H), 7.99 – 7.89 (m, 2H), 7.84 (d, $J = 8.3$ Hz, 1H), 7.72 – 7.63 (m, 1H), 7.60 (d, $J = 8.0$ Hz, 1H), 7.55 – 7.46 (m, 5H), 7.40 – 7.31 (m, 5H), 7.23 (t, $J = 8.0$ Hz, 3H), 5.36 (s, 2H), 2.69 (s, 3H). ^{13}C NMR (101 MHz, CDCl_3): $\delta = 192.3$ (1C), 152.9 (1C), 150.8 (1C), 139.0 (1C), 138.5 (1C), 138.3 (1C), 137.4 (1C), 134.0 (1C), 131.4 (1C), 131.3 (1C), 130.9 (1C), 130.3 (1C), 128.4 (1C), 127.5 (2C), 127.3 (1C), 127.0 (1C), 126.6 (1C), 126.5 (1C), 126.1 (1C), 126.1 (1C), 124.7 (1C), 124.2 (1C), 123.7 (2C), 123.3 (1C), 123.2 (1C), 121.4 (1C), 118.5 (1C), 115.5 (1C), 110.5 (1C), 50.8 (1C), 17.6 (1C) ppm. t_{R} (min) = 10.72 (*cis*) + 12.14 (*trans*), purity = 98.8%. MS: $[\text{M}+\text{H}]^+$ calc. for $[\text{C}_{33}\text{H}_{25}\text{N}_3\text{O}]^+$ = 480.58, found 480.25. High-Resolution Mass: m/z calcd for $\text{C}_{33}\text{H}_{26}\text{N}_3\text{O}$, 480.2070; found, 480.2065.

(E)-1-(5-fluoropentyl)-1H-indol-3-yl(3-(phenyldiazenyl)phenyl)methanone (18). Compound **17a** (89 mg, 0.27 mmol, 1eq) was dissolved in AcOH: TFA (6:1). Then, nitrosobenzene **11a** (89 mg, 0.82 mmol, 3 eq.) was added. The reaction mixture was stirred at 60°C for 4h. After completing the reaction, was diluted with EtOAc and washed with water and brine. The organic phases were collected, dried over Na_2SO_4 and concentrated. The black solid was purified by column chromatography (petroleum ether: EtOAc, 5:1) to afford the title compound (**18**) as a dark red oil. (19 mg, 17%). ^1H NMR (400 MHz, CDCl_3): $\delta = 8.50$ – 8.44 (m, 1H), 8.35 (t, $J = 1.7$ Hz, 1H), 8.13 – 8.08 (m, 1H), 7.97 – 7.91 (m, 3H), 7.65 (dd, $J = 9.7, 5.8$ Hz, 1H), 7.62 (s, 1H), 7.56 – 7.49 (m, 3H), 7.43 – 7.40 (m, 1H), 7.38 – 7.34 (m, 2H), 4.47 (dd, $J = 10.9, 5.0$ Hz, 1H), 4.36 (dd, $J = 10.8, 5.0$ Hz, 1H), 4.20 (t, $J = 7.1$ Hz, 2H), 2.01 – 1.89 (m, 2H), 1.79 – 1.64 (m, 2H), 1.54 – 1.42 (m, 2H). ^{13}C NMR (101 MHz, CDCl_3): $\delta = 190.4$ (1C), 153.0 (1C), 152.9 (1C), 142.4 (1C), 137.4 (1C), 137.3 (1C), 131.8 (1C), 131.4 (1C), 129.7 (1C), 129.6 (2C), 127.8 (1C), 125.6 (1C), 124.2 (1C), 123.5 (1C), 123.4 (2C), 123.4 (1C), 123.3 (1C), 116.1 (1C), 110.3 (1C), 84.0 (1C), 47.6 (1C), 30.3

(1C), 30.0 (1C), 23.3 (1C). LC: t_{R} (min) = 10.18 (*cis*) + 11.07 (*trans*), purity = 98.7%. MS: m/z $[\text{M}+\text{H}]^+$ calc. for $(\text{C}_{26}\text{H}_{24}\text{FN}_3\text{O})^+$ = 414.20, found 414.15. High-Resolution Mass: m/z calcd for $\text{C}_{26}\text{H}_{25}\text{FN}_3\text{O}$, 414.1976; found, 414.1976.

1-(5-Fluoropentyl)-3-{4-[(1E)-2-phenyldiazen-1-yl]benzoyl}-1H-indole (19a). Compound **17b** (111 mg, 0.34 mmol, 1eq.) was dissolved in AcOH: toluene : TFA (6:6:1). Then, nitrosobenzene **11a** was added (110mg, 1.02 mmol, 3 eq.). The reaction mixture was stirred at 60°C and monitored by TLC until the end of reagents. After the reaction was completed, the mixture was diluted with EtOAc and washed with water and brine. The organic phases were collected and dried over Na_2SO_4 . Lately, the product was purified by column chromatography (petroleum ether: EtOAc / 5:1) to afford the target compound (**19a**), as orange oil. (26 mg, 18%). ^1H NMR (400 MHz, CDCl_3): $\delta = 8.48$ – 8.41 (m, 1H), 8.03 (d, $J = 8.4$ Hz, 2H), 8.00 – 7.95 (m, 4H), 7.61 (s, 1H), 7.58 – 7.49 (m, 3H), 7.44 – 7.33 (m, 3H), 4.43 (dt, $J = 47.2, 5.8$ Hz, 2H), 4.20 (t, $J = 7.1$ Hz, 2H), 1.99 – 1.91 (m, 2H), 1.72 (ddt, $J = 13.7, 11.8, 5.9$ Hz, 2H), 1.53 – 1.44 (m, 2H). ^{13}C NMR (101 MHz, CDCl_3): $\delta = 190.5$ (1C), 154.5 (1C), 153.1 (1C), 143.1 (1C), 137.3 (1C), 132.0 (1C), 130.1 (2C), 129.6 (2C), 127.8 (1C), 124.2 (1C), 123.5 (2C), 123.4 (1C), 123.3 (1C), 123.2 (2C), 116.2 (1C), 110.3 (1C), 84.0 (1C), 47.6 (1C), 30.4 (1C), 30.2 (1C), 30.0 (1C), 23.4 (1C). LC: t_{R} (min) = 10.19 (*cis*) + 10.99 (*trans*), purity = 98.8%. MS: m/z $[\text{M}+\text{H}]^+$ calc. for $(\text{C}_{26}\text{H}_{24}\text{FN}_3\text{O})^+$ = 414.50, found 414.15. High-Resolution Mass: m/z calcd for $\text{C}_{26}\text{H}_{24}\text{FN}_3\text{O}$, 414.1976; found, 414.1997.

1-(5-Fluoropentyl)-3-{4-[(1E)-2-(4-methylphenyl)diazen-1-yl]benzoyl}-1H-indole (19c). Compound **17b** (100 mg, 0.31 mmol, eq.) was dissolved in AcOH: toluene : TFA (6:6:1). Then, nitroso compound **11c** was added (1.84 mmol, 6 eq.). The reaction mixture was stirred at 60°C and monitored by TLC until the end of reagents. After the reaction was completed, the mixture was diluted with ethyl acetate and washed with water and brine. The organic phases were collected and dried over Na_2SO_4 . Lately, the product was purified by column chromatography (petroleum ether: EtOAc / 5:1) to afford the target compound (**19c**), as orange solid. (29 mg, 22%). m.p. 131°C. ^1H NMR (400 MHz, CDCl_3): $\delta = 8.47$ – 8.29 (m, 1H), 7.98 (q, $J = 8.5$ Hz, 4H), 7.88 (d, $J = 8.2$ Hz, 2H), 7.60 (s, 1H), 7.44 – 7.30 (m, 5H), 4.43 (dt, $J = 47.3, 5.8$ Hz, 2H), 4.22 – 4.16 (m, 2H), 2.46 (s, 3H), 1.95 (dt, $J = 15.0, 7.3$ Hz, 2H), 1.81 – 1.64 (m, 2H), 1.54 – 1.42 (m, 2H). ^{13}C NMR (101 MHz, CDCl_3): $\delta = 190.2$ (1C), 154.3 (1C), 150.9 (1C), 142.5 (1C), 142.4 (1C), 137.0 (2C), 130.0 (2C), 129.8 (2C), 127.4 (1C), 123.9 (1C), 123.2 (2C), 123.0 (1C), 122.9 (1C), 122.7 (2C), 115.9 (1C), 110.0 (1C), 83.7 (1C), 47.2 (1C), 30.0 (1C), 29.7 (1C), 23.0 (1C), 21.7 (1C). LC: t_{R} (min) = 10.37 (*cis*) + 11.23 (*trans*), purity = 98.9%. MS: m/z $[\text{M}+\text{H}]^+$ calc. for $(\text{C}_{27}\text{H}_{26}\text{FN}_3\text{O})^+$ = 428.53, found 428.20. High-Resolution Mass: m/z calcd for $\text{C}_{27}\text{H}_{26}\text{FN}_3\text{O}$, 427.2054; found, 427.2057.

(E)-1-(5-fluoropentyl)-N-(2-(phenyldiazenyl)benzyl)-1H-indole-3-carboxamide (27a). To a suspension of NaH (10.54 mg, 0.25 mmol, 3eq) in DMF was added compound **26a** (29 mg, 0.081 mmol, 1eq). After stirring at room temperature for 30 min, 1-bromo-5-fluoropentane (33 μL , 0.25 mmol, 3eq) was added dropwise. The resulting mixture was heated at 65°C for 3h. After reaction, the mixture was diluted with ethyl acetate and washed with water and brine.

The organic layer was dried over Na₂SO₄ and concentrated in vacuo. The crude product was purified by column chromatography using (petroleum ether: ethyl acetate, 3:1) to afford the target compound (**27a**), as orange solid. (15 mg, 41%). m.p. 163 °C. ¹H NMR (400 MHz, CDCl₃): δ = 7.99 – 7.95 (m, 2H), 7.80 – 7.72 (m, 2H), 7.67 (d, *J* = 6.2 Hz, 2H), 7.57 – 7.51 (m, 3H), 7.49 – 7.37 (m, 2H), 7.31 (dt, *J* = 8.3, 0.9 Hz, 1H), 7.21 – 7.13 (m, 1H), 7.00 – 6.89 (m, 1H), 6.69 (t, *J* = 6.2 Hz, 1H), 5.19 (d, *J* = 6.0 Hz, 2H), 4.44 (t, *J* = 6.0 Hz, 1H), 4.32 (t, *J* = 5.9 Hz, 1H), 4.09 (t, *J* = 7.1 Hz, 2H), 1.92 – 1.82 (m, 2H), 1.73 – 1.62 (m, 2H), 1.44 – 1.37 (m, 2H). ¹³C NMR (101 MHz, CDCl₃): δ = 165.3 (1C), 153.3 (1C), 150.8 (1C), 138.4 (1C), 136.9 (1C), 132.2 (1C), 132.1 (1C), 131.8 (1C), 130.8 (1C), 129.7 (2C), 128.8 (1C), 125.6 (1C), 123.5 (2C), 122.8 (1C), 121.7 (1C), 120.5 (1C), 116.7 (1C), 111.4 (1C), 110.6 (1C), 84.1 (1C), 47.1 (1C), 40.8 (1C), 30.4 (1C), 30.0 (1C), 23.2 (1C). LC: t_R (min) = 9.87 (*cis*) + 10.68 (*trans*), purity = 99.1%. MS: *m/z* [M+H]⁺ calc. for (C₂₇H₂₇FN₄O)⁺ = 443.22, found 443.20. High-Resolution Mass: *m/z* calcd for C₂₇H₂₈FN₄O, 443.2242; found, 443.2257.

(E)-1-(5-fluoropentyl)-N-(3-(phenyldiazenyl)benzyl)-1H-indole-3-carboxamide (27b). To a suspension of NaH (15.2 mg, 0.36 mmol, 1.3 eq) in DMF was added compound **26b** (100mg, 0.28 mmol, 1eq). After stirring at room temperature for 30 min, 1-bromo-5-fluoropentane (75 μL, 0.75 mmol, 3eq) was added dropwise. The resulting mixture was heated at 65°C for 3h. After reaction, the mixture was diluted with ethyl acetate and washed with water and brine. The organic layer was dried over Na₂SO₄ and concentrated in vacuo. The crude product was purified by flash chromatography (water: methanol, 95:5 → 5:95) to afford the title product (**27b**) as an orange solid. (40 mg, 32%). m.p. 130–131 °C. ¹H NMR (400 MHz, CDCl₃): δ = 7.93 (dd, *J* = 21.0, 8.8 Hz, 4H), 7.85 (d, *J* = 7.4 Hz, 1H), 7.76 (s, 1H), 7.56 – 7.44 (m, 5H), 7.38 (d, *J* = 8.0 Hz, 1H), 7.31 – 7.22 (m, 2H), 6.37 (s, 1H), 4.82 (s, 2H), 4.41 (dt, *J* = 47.2, 5.9 Hz, 2H), 4.15 (t, *J* = 7.0 Hz, 2H), 1.97 – 1.86 (m, 2H), 1.78 – 1.63 (m, 2H), 1.45 (dt, *J* = 18.7, 7.7 Hz, 2H). ¹³C NMR (101 MHz, CDCl₃): δ = 165.3 (1C), 153.1 (1C), 152.8 (1C), 140.3 (1C), 136.7 (1C), 131.7 (1C), 131.2 (1C), 130.5 (1C), 129.7 (1C), 129.2 (2C), 125.6 (1C), 123.0 (2C), 122.7 (1C), 122.3 (1C), 122.0 (1C), 121.7 (1C), 120.4 (1C), 110.8 (1C), 110.4 (1C), 83.8 (1C), 46.9 (1C), 43.5 (1C), 30.0 (1C), 29.8 (1C), 22.9 (1C). LC: t_R (min) = 9.72 (*cis*) + 10.56 (*trans*), purity = 97.9%. MS: *m/z* [M+H]⁺ calc. for (C₂₇H₂₇FN₄O)⁺ = 443.22, found 443.20. High-Resolution Mass: *m/z* calcd for C₂₇H₂₈FN₄O, 443.2242; found, 443.2226.

(E)-1-(5-fluoropentyl)-N-(4-(phenyldiazenyl)benzyl)-1H-indole-3-carboxamide (27c). To a suspension of NaH (31.6 mg, 0.75 mmol, 3eq) in DMF was added compound **26c** (90mg, 0.25 mmol, 1eq). After stirring at room temperature for 30 min, 1-bromo-5-fluoropentane (100 μL, 0.75 mmol, 3eq) was added dropwise. The resulting mixture was heated at 65°C for 3h. After reaction, the mixture was diluted with ethyl acetate and washed with water and brine. The organic layer was dried over Na₂SO₄ and concentrated in vacuo. The crude product was purified by column chromatography using (petroleum ether: ethyl acetate, 2:1) to afford the title product (**27c**) as an orange solid. (52 mg, 48 %). m.p. 129 °C. ¹H NMR δ = 7.98 – 7.89 (m, 5H), 7.75 (s, 1H), 7.58 – 7.45 (m, 5H), 7.39 (d, *J* = 7.5 Hz, 1H), 7.32 – 7.22 (m,

3H), 4.79 (d, *J* = 5.2 Hz, 2H), 4.50 – 4.33 (m, 2H), 4.16 (t, *J* = 7.1 Hz, 2H), 1.97 – 1.88 (m, 2H), 1.75 (dd, *J* = 14.2, 7.0 Hz, 1H), 1.72 – 1.64 (m, 1H), 1.46 (ddd, *J* = 18.8, 9.1, 6.4 Hz, 2H). ¹³C NMR (101 MHz, CDCl₃): δ = 165.0 (1C), 152.5 (1C), 151.8 (1C), 141.9 (1C), 136.4 (1C), 131.4 (1C), 130.8 (1C), 128.9 (2C), 128.2 (2C), 125.2 (1C), 123.1 (2C), 122.7 (2C), 122.4 (1C), 121.4 (1C), 120.0 (1C), 110.5 (1C), 110.1 (1C), 83.5 (1C), 46.6 (1C), 43.0 (1C), 29.9 (1C), 29.6 (1C), 22.7. (1C). LC: t_R (min) = 9.76 (*cis*) + 10.57 (*trans*), purity = 95.20%. MS: *m/z* [M+H]⁺ calc. for (C₂₇H₂₇FN₄O)⁺ = 443.22, found 443.20. High-Resolution Mass: *m/z* calcd for C₂₇H₂₈FN₄O, 443.2242; found, 443.2231.

(E)-1-(3-fluoropropyl)-N-(2-(phenyldiazenyl)benzyl)-1H-indole-3-carboxamide (28a). Protocol I: To a suspension of NaH (11.37 mg, 0.27 mmol, 3eq) in DMF was added compound **26a** (33 mg, 0.09 mmol, 1eq). After stirring at room temperature for 30 min, 3-fluoropropyl 4-methylbenzenesulfonate (63 mg, 0.27 mmol, 3eq) was added dropwise. The resulting mixture was heated at 65°C for 3h. After reaction, the mixture was diluted with ethyl acetate and washed with water and brine. The organic layer was dried over Na₂SO₄ and concentrated in vacuo. Protocol II: The reaction was carried out according to general procedure I, using compound **34** (50 mg, 0.16 mmol, 1 eq) and nitrosobenzene (24 mg, 0.22 mmol, 1.4 eq). The crude product was purified to afford the title product (**28a**) as an orange solid. (47 mg, 71%). m.p. 151 °C. ¹H NMR (400 MHz, CDCl₃): δ = 7.99 – 7.93 (m, 2H), 7.80 – 7.74 (m, 2H), 7.71 (s, 1H), 7.66 (dd, *J* = 7.4, 1.5 Hz, 1H), 7.57 – 7.50 (m, 3H), 7.47 (td, *J* = 7.4, 1.4 Hz, 1H), 7.40 (td, *J* = 7.6, 1.6 Hz, 1H), 7.34 (d, *J* = 8.3 Hz, 1H), 7.20 (ddd, *J* = 8.3, 7.1, 1.1 Hz, 1H), 6.98 (td, *J* = 7.5, 1.0 Hz, 1H), 6.82 (s, 1H), 5.18 (s, 2H), 4.41 (t, *J* = 5.5 Hz, 1H), 4.27 (dt, *J* = 13.5, 6.1 Hz, 3H), 2.23 – 2.08 (m, 2H). ¹³C NMR (101 MHz, CDCl₃): δ = 164.9 (1C), 153.0 (1C), 150.5 (1C), 137.9 (1C), 136.7 (1C), 132.0 (1C), 131.8 (1C), 131.5 (1C), 130.6 (1C), 129.4 (2C), 128.5 (1C), 125.3 (1C), 123.2 (2C), 122.8 (1C), 121.6 (1C), 120.3 (1C), 116.4 (1C), 111.3 (1C), 110.2 (1C), 80.4 (1C), 42.5 (1C), 40.5 (1C), 30.9 (1C). t_R (min) = 9.51 (*cis*) + 10.43 (*trans*), purity = 97.6%. MS: *m/z* [M+H]⁺ calc. for (C₂₅H₂₃FN₄O)⁺ = 415.19, found 415.20. High-Resolution Mass: *m/z* calcd for C₂₅H₂₃FN₄NaO, 437.1748; found, 437.1749.

(E)-1-(3-fluoropropyl)-N-(3-(phenyldiazenyl)benzyl)-1H-indole-3-carboxamide (28b). To a suspension of NaH (52.7 mg, 1.25 mmol, 3 eq) in DMF was added compound **26b** (150mg, 0.42 mmol, 1eq). After stirring at room temperature for 30 min, 3-fluoropropyl 4-methylbenzenesulfonate (290 mg, 1.25 mmol, 3eq) was added dropwise. The resulting mixture was heated at 65°C for 3h. After reaction, the mixture was diluted with ethyl acetate and washed with water and brine. The organic layer was dried over Na₂SO₄ and concentrated in vacuo. The crude product was purified by flash chromatography (water: methanol, 95:5 → 5:95) to afford the title product (**28b**) as an orange solid. (33 mg, 19%). m.p. 141 °C. ¹H NMR (400 MHz, CDCl₃): δ = 8.00 (d, *J* = 7.6 Hz, 1H), 7.92 (dd, *J* = 9.7, 8.5 Hz, 3H), 7.85 (d, *J* = 7.4 Hz, 1H), 7.75 (s, 1H), 7.57 – 7.44 (m, 5H), 7.40 (d, *J* = 8.1 Hz, 1H), 7.32 – 7.23 (m, 2H), 6.38 (s, 1H), 4.83 (d, *J* = 5.8 Hz, 2H), 4.48 (t, *J* = 5.4 Hz, 1H), 4.37 – 4.28 (m, 3H), 2.28 – 2.13 (m, 2H). ¹³C NMR (101 MHz, CDCl₃): δ = 165.2 (1C), 153.1 (1C), 152.8 (1C), 140.2 (1C), 136.7 (1C), 131.5 (1C), 131.2 (1C), 130.5

(1C), 129.6 (1C), 129.2 (2C), 125.7 (1C), 123.0 (2C), 122.9 (1C), 122.3 (1C), 122.0 (1C), 121.8 (1C), 120.6 (1C), 111.2 (1C), 110.2 (1C), 80.4 (1C), 43.4 (1C), 42.7 (1C), 30.9 (1C). LC: t_R (min) = 9.38 (*cis*) + 10.36 (*trans*), purity = 99.5%. MS: m/z [M+H]⁺ calc. for (C₂₅H₂₃FN₄O)⁺ = 415.19, found 415.15. High-Resolution Mass: m/z calcd for C₂₅H₂₄FN₄O, 415.1929; found, 415.1934.

(E)-1-(3-fluoropropyl)-N-(4-(phenyldiazenyl)benzyl)-1H-indole-3-carboxamide (28c). To a suspension of NaH (26.1 mg, 0.62 mmol, 3 eq) in DMF was added compound **26c** (74 mg, 0.21 mmol, 1eq). After stirring at room temperature for 30 min, 3-fluoropropyl 4-methylbenzenesulfonate (144 mg, 0.62 mmol, 3 eq) was added dropwise. The resulting mixture was heated at 65°C for 3h. After reaction, the mixture was diluted with ethyl acetate and washed with water and brine. The organic layer was dried over Na₂SO₄ and concentrated in vacuo. The crude product was purified by flash chromatography (water: methanol, 95:5 → 5:95) to afford the title product (**28c**) as an orange solid. (25 mg, 29%). m.p. 120 °C. ¹H NMR (400 MHz, CDCl₃): δ = 7.97 (d, J = 7.3 Hz, 1H), 7.91 (d, J = 8.1 Hz, 4H), 7.76 (s, 1H), 7.58 – 7.44 (m, 5H), 7.41 (d, J = 7.8 Hz, 1H), 7.33 – 7.23 (m, 2H), 6.33 (s, 1H), 4.79 (s, 2H), 4.47 (t, J = 5.5 Hz, 1H), 4.38 – 4.30 (m, 3H), 2.31 – 2.22 (m, 1H), 2.18 (dd, J = 11.9, 6.1 Hz, 1H). ¹³C NMR (101 MHz, CDCl₃): δ = 165.2 (1C), 152.8 (1C), 152.2 (1C), 142.1 (1C), 136.7 (1C), 131.6 (1C), 131.2 (1C), 129.2 (2C), 128.6 (2C), 125.6 (1C), 123.4 (2C), 123.0 (3C), 121.9 (1C), 120.5 (1C), 111.2 (1C), 110.3 (1C), 80.4 (1C), 43.4 (1C), 42.7 (1C), 30.9 (1C). LC: t_R (min) = 9.43 (*cis*) + 10.38 (*trans*), purity = 98.5%. MS: m/z [M+H]⁺ calc. for (C₂₅H₂₃FN₄O)⁺ = 415.19, found 415.20. High-Resolution Mass: m/z calcd for C₂₅H₂₄FN₄O, 415.1929; found, 415.1936.

(E)-1-(3-fluoropropyl)-N-(2-(o-tolyldiazenyl)benzyl)-1H-indole-3-carboxamide (36b). The reaction was carried out according to general procedure I, using compound **34** (50 mg, 0.16 mmol, 1 eq) and 2-nitrosotoluene (24 mg, 0.22 mmol, 1.4 eq). The crude product was purified to afford the title product (**36b**) as an orange solid. (47 mg, 71%). m.p. 151 °C. ¹H NMR (400 MHz, CDCl₃): δ = 7.76 (td, J = 8.5, 1.2 Hz, 2H), 7.68 – 7.64 (m, 3H), 7.45 (td, J = 7.4, 1.4 Hz, 1H), 7.42 – 7.36 (m, 3H), 7.34 (d, J = 8.3 Hz, 1H), 7.28 (dd, J = 8.3, 2.5 Hz, 1H), 7.20 (td, J = 7.1, 1.0 Hz, 1H), 6.97 (td, J = 7.1, 1.0 Hz, 1H), 6.78 (s, 1H), 5.20 (d, J = 5.7 Hz, 2H), 4.41 (t, J = 5.4 Hz, 1H), 4.29 (t, J = 5.4 Hz, 1H), 4.25 (t, J = 6.8 Hz, 2H), 2.76 (s, 3H), 2.23 – 2.07 (m, 2H). ¹³C NMR (101 MHz, CDCl₃): δ = 164.9 (1C), 151.1 (1C), 150.8 (1C), 138.8 (1C), 138.1 (1C), 136.6 (1C), 131.9 (1C), 131.6 (1C), 131.6 (1C), 131.5 (1C), 130.5 (1C), 128.4 (1C), 126.7 (1C), 125.3 (1C), 122.7 (1C), 121.6 (1C), 120.3 (1C), 116.3 (1C), 115.7 (1C), 111.4 (1C), 110.2 (1C), 80.4 (1C), 42.5 (1C), 40.61 (1C), 30.9 (1C), 17.8 (1C). t_R (min) = 9.81 (*cis*) + 10.76 (*trans*), purity = 98.4%. MS: m/z [M+H]⁺ calc. for (C₂₆H₂₅FN₄O)⁺ = 429.21, found 429.20. High-Resolution Mass: m/z calcd for C₂₆H₂₆FN₄O, 429.2085; found, 429.2086.

(E)-1-(3-fluoropropyl)-N-(2-(p-tolyldiazenyl)benzyl)-1H-indole-3-carboxamide (36c). The reaction was carried out according to general procedure I, using compound **34** (34 mg, 0.1 mmol, 1 eq) and nitroso compound **11c** (0.6 mmol, 6 eq). The crude product was purified to afford the title product (**36c**) as an orange solid. (28 mg, 73%). m.p. 132 °C. ¹H NMR (400 MHz, CDCl₃): δ = 7.87 (d, J = 8.3 Hz,

2H), 7.81 – 7.72 (m, 2H), 7.70 (s, 1H), 7.65 (dd, J = 7.5, 1.6 Hz, 1H), 7.47 – 7.37 (m, 2H), 7.34 (dd, J = 8.3, 3.4 Hz, 3H), 7.21 (ddd, J = 8.3, 7.0, 1.1 Hz, 1H), 7.02 – 6.97 (m, 1H), 6.79 (s, 1H), 5.16 (s, 2H), 4.41 (t, J = 5.5 Hz, 1H), 4.32 – 4.23 (m, 3H), 2.46 (s, 3H), 2.19 (q, J = 5.3 Hz, 1H), 2.12 (q, J = 5.1 Hz, 1H). ¹³C NMR (101 MHz, CDCl₃): δ = 164.6 (1C), 150.8 (1C), 150.2 (1C), 141.9 (1C), 137.2 (1C), 136.4 (1C), 131.6 (1C), 131.2 (1C), 130.2 (1C), 129.8 (2C), 128.2 (1C), 125.0 (1C), 122.9 (2C), 122.4 (1C), 121.3 (1C), 120.0 (1C), 116.1 (1C), 110.0 (1C), 109.9 (1C), 80.1 (1C), 42.2 (1C), 40.2 (1C), 30.6 (1C), 21.4 (1C). t_R (min) = 9.75 (*cis*) + 10.67 (*trans*), purity = 98.9%. MS: m/z [M+H]⁺ calc. for (C₂₆H₂₅FN₄O)⁺ = 429.21, found 429.15. High-Resolution Mass: m/z calcd for C₂₆H₂₅FN₄NaO, 451.1905; found, 451.1903.

(E)-N-(2-((4-ethylphenyl)diazenyl)benzyl)-1-(3-fluoropropyl)-1H-indole-3-carboxamide (36d). The reaction was carried out according to general procedure I, using compound **34** (59 mg, 0.19 mmol, 1 eq) and nitroso compound **11d** (1.12 mmol, 6 eq). The crude product was purified to afford the title product (**36d**) as an orange solid. (52 mg, 62%). m.p. 126 °C. ¹H NMR (400 MHz, CDCl₃): δ = 7.89 (d, J = 8.3 Hz, 2H), 7.80 – 7.72 (m, 2H), 7.70 (s, 1H), 7.65 (dd, J = 7.5, 1.6 Hz, 1H), 7.47 – 7.39 (m, 2H), 7.35 (t, J = 8.4 Hz, 3H), 7.20 (ddd, J = 8.3, 7.0, 1.1 Hz, 1H), 6.97 (t, J = 7.6 Hz, 1H), 6.80 (s, 1H), 5.16 (s, 2H), 4.41 (t, J = 5.5 Hz, 1H), 4.33 – 4.21 (m, 3H), 2.75 (q, J = 7.6 Hz, 2H), 2.23 – 2.08 (m, 2H), 1.31 (t, J = 7.6 Hz, 3H). ¹³C NMR (101 MHz, CDCl₃): δ = 164.9 (1C), 151.3 (1C), 150.68 (1C), 148.5 (1C), 137.6 (1C), 136.7 (1C), 131.9 (1C), 131.4 (1C), 130.5 (1C), 128.9 (2C), 128.5 (1C), 125.3 (1C), 123.3 (2C), 122.7 (1C), 121.6 (1C), 120.3 (1C), 116.4 (1C), 111.5 (1C), 110.2 (1C), 80.4 (1C), 42.5 (1C), 40.6 (1C), 30.9 (1C), 29.0 (1C), 15.6 (1C). t_R (min) = 9.98 (*cis*) + 10.87 (*trans*), purity = 97.3%. MS: m/z [M+H]⁺ calc. for (C₂₇H₂₇FN₄O)⁺ = 443.22, found 443.25. High-Resolution Mass: m/z calcd for C₂₇H₂₈FN₄O, 443.2242; found, 443.2239.

(E)-N-(2-((3-ethylphenyl)diazenyl)benzyl)-1-(3-fluoropropyl)-1H-indole-3-carboxamide (36e). The reaction was carried out according to general procedure I, using compound **34** (59 mg, 0.19 mmol, 1 eq) and nitroso compound **11e** (1.12 mmol, 6 eq). The crude product was purified to afford the title product (**36e**) as an orange solid. (55 mg, 65%). m.p. 123 °C. ¹H NMR (400 MHz, CDCl₃): δ = 7.81 – 7.74 (m, 4H), 7.70 (s, 1H), 7.66 (dd, J = 7.5, 1.6 Hz, 1H), 7.49 – 7.39 (m, 3H), 7.39 – 7.32 (m, 2H), 7.20 (ddd, J = 8.3, 7.1, 1.1 Hz, 1H), 6.97 (ddd, J = 8.0, 7.1, 1.0 Hz, 1H), 6.80 (s, 1H), 5.18 (s, 2H), 4.41 (t, J = 5.4 Hz, 1H), 4.32 – 4.23 (m, 3H), 2.74 (q, J = 7.6 Hz, 2H), 2.19 (p, J = 6.4 Hz, 1H), 2.12 (p, J = 6.2 Hz, 1H), 1.27 (t, J = 7.6 Hz, 3H). ¹³C NMR (101 MHz, CDCl₃): δ = 164.7 (1C), 153.0 (1C), 150.4 (1C), 145.6 (1C), 137.6 (1C), 136.5 (1C), 131.8 (1C), 131.5 (1C), 131.1 (1C), 130.4 (1C), 129.2 (1C), 128.4 (1C), 125.2 (1C), 122.7 (1C), 122.6 (1C), 121.4 (1C), 120.2 (1C), 120.1 (1C), 116.3 (1C), 111.3 (1C), 110.0 (1C), 80.2 (1C), 42.4 (1C), 40.4 (1C), 30.8 (1C), 28.8 (1C), 15.5 (1C). t_R (min) = 10.00 (*cis*) + 10.86 (*trans*), purity = 97.7%. MS: m/z [M+H]⁺ calc. for (C₂₇H₂₇FN₄O)⁺ = 443.22, found 443.20. High-Resolution Mass: m/z calcd for C₂₇H₂₈FN₄O, 443.2242; found, 443.2246.

(E)-1-(5-fluoropentyl)-N-(2-(o-tolyldiazenyl)benzyl)-1H-indole-3-carboxamide (37b). The reaction was carried out according to general procedure I, using compound **35** (51 mg, 0.14 mmol, 1 eq) and 2-nitrosotoluene (24 mg, 0.22

mmol, 1.4 eq). The crude product was purified to afford the title product (**37b**) as an orange solid. (7 mg, 11%). m.p. 162 °C. ¹H NMR (400 MHz, CDCl₃): δ = 7.77 – 7.71 (m, 2H), 7.69 – 7.63 (m, 2H), 7.46 (td, J = 7.4, 1.4 Hz, 1H), 7.42 – 7.38 (m, 2H), 7.33 – 7.28 (m, 1H), 7.22 – 7.14 (m, 1H), 6.95 (t, J = 7.6 Hz, 1H), 6.76 (s, 1H), 5.20 (d, J = 6.1 Hz, 2H), 4.44 (t, J = 5.8 Hz, 1H), 4.32 (t, J = 5.8 Hz, 1H), 4.16 – 4.05 (m, 2H), 2.76 (s, 3H), 1.86 (p, J = 7.6 Hz, 2H), 1.75 – 1.59 (m, 4H), 1.46 – 1.35 (m, 3H). ¹³C NMR (101 MHz, CDCl₃): δ = 165.3 (1C), 151.4 (1C), 151.1 (1C), 139.1 (1C), 138.5 (1C), 136.9 (1C), 132.2 (1C), 132.0 (1C), 131.9 (1C), 131.8 (1C), 130.8 (1C), 128.7 (1C), 127.0 (1C), 125.6 (1C), 122.8 (1C), 121.7 (1C), 120.5 (1C), 116.6 (1C), 116.0 (1C), 111.5 (1C), 110.6 (1C), 84.1 (1C), 47.1 (1C), 40.9 (1C), 30.3 (1C), 30.0 (1C), 23.2 (1C), 18.1 (1C). t_R (min) = 9.96 (*cis*) + 10.82 (*trans*), purity = 96.8%. MS: m/z [M+H]⁺ calc. for (C₂₈H₂₉FN₄O)⁺ = 457.24, found 457.20. High-Resolution Mass: m/z calcd for C₂₈H₂₉FN₄NaO, 479.2218; found, 479.2218.

(E)-1-(5-fluoropentyl)-N-(2-(p-tolyldiazenyl)benzyl)-1H-indole-3-carboxamide (37c). The reaction was carried out according to general procedure I, using compound **35** (34 mg, 0.1 mmol, 1 eq) and nitroso compound **11c** (0.6 mmol, 6 eq). The crude product was purified to afford the title product (**37c**) as an orange solid. (20 mg, 44%). m.p. 132 °C. ¹H NMR (400 MHz, CDCl₃): δ = 7.93 – 7.77 (m, 2H), 7.68 (dt, J = 8.1, 2.6 Hz, 2H), 7.61 – 7.46 (m, 2H), 7.40 – 7.28 (m, 2H), 7.25 (t, J = 7.9 Hz, 3H), 7.14 – 7.06 (m, 1H), 6.96 – 6.85 (m, 1H), 6.65 (s, 1H), 5.10 (d, J = 6.0 Hz, 2H), 4.36 (t, J = 5.9 Hz, 1H), 4.25 (t, J = 5.8 Hz, 1H), 4.10 – 3.97 (m, 2H), 2.38 (s, 3H), 1.77 (p, J = 7.4 Hz, 2H), 1.70 – 1.51 (m, 2H), 1.32 (ddt, J = 12.8, 10.5, 6.2 Hz, 2H). ¹³C NMR (101 MHz, CDCl₃): δ = 186.4 (1C), 151.0 (1C), 150.4 (1C), 142.0 (1C), 137.6 (1C), 136.5 (1C), 136.5 (1C), 131.3 (1C), 130.4 (1C), 129.9 (2C), 128.3 (1C), 124.2 (1C), 123.1 (2C), 122.3 (1C), 121.2 (1C), 120.0 (1C), 116.2 (1C), 110.7 (1C), 110.1 (1C), 84.2 (1C), 46.6 (1C), 40.4 (1C), 29.9 (1C), 29.6 (1C), 22.8 (1C), 21.6 (1C). t_R (min) = 9.92 (*cis*) + 10.75 (*trans*), purity = 95.0%. MS: m/z [M+H]⁺ calc. for (C₂₈H₂₉FN₄O)⁺ = 457.24, found 457.20. High-Resolution Mass: m/z calcd for C₂₈H₃₀FN₄O, 457.2398; found, 457.2392.

(E)-N-(2-((4-ethylphenyl)diazenyl)benzyl)-1-(5-fluoropentyl)-1H-indole-3-carboxamide (37d). The reaction was carried out according to general procedure I, using compound **35** (72 mg, 0.19 mmol, 1 eq) and nitroso compound **11d** (1.12 mmol, 6 eq). The crude product was purified to afford the title product (**37d**) as an orange solid. (48 mg, 54%). m.p. 128 °C. ¹H NMR (400 MHz, CDCl₃): δ = 7.92 – 7.87 (m, 2H), 7.75 (td, J = 7.6, 1.3 Hz, 2H), 7.70 (s, 1H), 7.65 (dd, J = 7.5, 1.6 Hz, 1H), 7.47 – 7.38 (m, 2H), 7.38 – 7.34 (m, 2H), 7.31 (dt, J = 8.3, 0.9 Hz, 1H), 7.18 (ddd, J = 8.2, 7.1, 1.1 Hz, 1H), 6.95 (ddd, J = 8.1, 7.1, 1.0 Hz, 1H), 5.17 (s, 2H), 4.44 (t, J = 5.9 Hz, 1H), 4.32 (t, J = 5.9 Hz, 1H), 4.11 (dt, J = 16.8, 7.1 Hz, 2H), 2.76 (q, J = 7.6 Hz, 2H), 1.91 – 1.79 (m, 2H), 1.76 – 1.58 (m, 2H), 1.46 – 1.35 (m, 2H), 1.31 (t, J = 7.6 Hz, 3H). ¹³C NMR (101 MHz, CDCl₃): δ = 165.0 (1C), 151.3 (1C), 150.6 (1C), 148.5 (1C), 137.7 (1C), 136.6 (1C), 132.0 (1C), 131.5 (1C), 130.5 (1C), 128.9 (2C), 128.5 (1C), 125.3 (1C), 123.3 (2C), 122.4 (1C), 121.4 (1C), 120.2 (1C), 116.4 (1C), 111.0 (1C), 110.3 (1C), 83.8 (1C), 46.8 (1C), 40.5 (1C), 30.0 (1C), 29.7 (1C), 29.0 (1C), 22.9 (1C), 15.6 (1C). t_R (min) = 10.20 (*cis*) + 10.99 (*trans*), purity = 96.9%. MS: m/z [M+H]⁺ calc.

for (C₂₉H₃₁FN₄O)⁺ = 471.26, found 471.25. High-Resolution Mass: m/z calcd for C₂₉H₃₂FN₄O, 471.2555; found, 471.2570.

(E)-N-(2-((3-ethylphenyl)diazenyl)benzyl)-1-(5-fluoropentyl)-1H-indole-3-carboxamide (37e). The reaction was carried out according to general procedure I, using compound **35** (72 mg, 0.19 mmol, 1 eq) and nitroso compound **11e** (1.12 mmol, 6 eq). The crude product was purified to afford the title product (**37e**) as an orange solid. (30 mg, 34%). m.p. 138 °C. ¹H NMR (400 MHz, CDCl₃): δ = 7.80 (p, J = 1.8 Hz, 1H), 7.75 (ddd, J = 7.7, 6.2, 1.3 Hz, 2H), 7.66 (d, J = 6.3 Hz, 2H), 7.48 – 7.42 (m, 2H), 7.41 (dd, J = 7.7, 1.6 Hz, 1H), 7.39 – 7.34 (m, 1H), 7.31 (d, J = 8.3 Hz, 1H), 7.25 – 7.09 (m, 2H), 7.01 – 6.93 (m, 1H), 6.73 (s, 1H), 5.18 (d, J = 6.0 Hz, 2H), 4.44 (td, J = 5.9, 3.7 Hz, 1H), 4.33 (td, J = 6.0, 3.7 Hz, 1H), 4.14 – 4.06 (m, 2H), 2.74 (q, J = 7.6 Hz, 2H), 1.85 (p, J = 7.2 Hz, 2H), 1.74 – 1.60 (m, 2H), 1.46 – 1.35 (m, 2H), 1.27 (t, J = 7.6 Hz, 3H). ¹³C NMR (101 MHz, CDCl₃): δ = 164.9 (1C), 153.2 (1C), 150.6 (1C), 145.7 (1C), 137.9 (1C), 136.7 (1C), 131.8 (1C), 131.6 (1C), 131.2 (1C), 130.5 (1C), 129.3 (1C), 128.4 (1C), 125.3 (1C), 122.8 (1C), 122.4 (1C), 121.4 (1C), 120.4 (1C), 120.2 (1C), 116.4 (1C), 111.2 (1C), 110.3 (1C), 83.7 (1C), 46.8 (1C), 40.5 (1C), 30.0 (1C), 29.7 (1C), 28.9 (1C), 22.9 (1C), 15.6 (1C). t_R (min) = 10.13 (*cis*) + 10.91 (*trans*), purity = 99.8%. MS: m/z [M+H]⁺ calc. for (C₂₉H₃₁FN₄O)⁺ = 471.26, found 471.25. High-Resolution Mass: m/z calcd for C₂₉H₃₂FN₄O, 471.2555; found, 471.2553.

(Z)-N-(11,12-dihydrodibenzo[c,g][1,2]diazocin-3-yl)-1-(5-fluoropentyl)-1H-indole-3-carboxamide (49). To a mixture of amine **48** (22 mg, 0.1 mmol, 1 eq), carboxylic acid **24** (34 mg, 0.14 mmol, 1.4 eq) and 2-chloro-1-methylpyridinium iodide (38 mg, 0.14 mmol, 1.4 eq) in DCM at 0 °C under argon atmosphere, was added DIPEA (54 μL, 0.3 mmol, 3 eq). The reaction mixture was allowed to warm to r.t. and stirred. After 4-24h (check by TLC), water was added, and the layers were separate. The aqueous layer was extracted with DCM. The combined organic layers were dried over Na₂SO₄ and concentrated in vacuo. The crude was purified by flash chromatography with isocratic gradient (hexane: AcOEt; 100:0→0:100) to afford the title compound (**49**) as an orange solid. (18 mg, 41%). m.p. 186 °C. ¹H NMR (400 MHz, CDCl₃): δ = 8.01 – 7.96 (m, 1H), 7.73 (s, 1H), 7.60 (s, 1H), 7.39 (dt, J = 8.3, 2.2 Hz, 2H), 7.33 – 7.27 (m, 2H), 7.17 – 7.11 (m, 2H), 7.06 – 6.99 (m, 2H), 6.97 (d, J = 8.3 Hz, 1H), 6.86 (dd, J = 7.7, 1.3 Hz, 1H), 4.47 (t, J = 5.8 Hz, 1H), 4.36 (t, J = 5.9 Hz, 1H), 4.17 (t, J = 7.1 Hz, 2H), 3.02 – 2.94 (m, 2H), 2.80 – 2.72 (m, 2H), 1.92 (p, J = 7.2 Hz, 2H), 1.79 – 1.62 (m, 2H), 1.49 – 1.40 (m, 2H). ¹³C NMR (101 MHz, CDCl₃): δ = 163.1 (1C), 155.9 (1C), 155.6 (1C), 137.3 (1C), 136.8 (1C), 131.7 (1C), 130.5 (1C), 129.8 (1C), 128.2 (1C), 127.3 (1C), 126.9 (1C), 125.5 (1C), 123.6 (1C), 123.0 (1C), 122.0 (1C), 120.3 (1C), 119.0 (1C), 118.6 (1C), 111.1 (1C), 110.5 (1C), 110.0 (1C), 83.8 (1C), 46.9 (1C), 31.8 (1C), 31.4 (1C), 29.9 (1C), 29.7 (1C), 23.0 (1C). t_R (min) = 9.93 (*Z*) + 10.28 (*E*), purity = 99.2%. MS: m/z [M+H]⁺ calc. for (C₂₈H₂₇FN₄O)⁺ = 455.22, found 455.20. High-Resolution Mass: m/z calcd for C₂₈H₂₈FN₄O, 455.2242; found, 455.2254.

(Z)-dibenzo[c,g][1,2,5]triazocin-11(12H)-yl(1-(5-fluoropentyl)-1H-indol-3-yl)methanone (51). To a mixture of amine **50** (20 mg, 0.09 mmol, 1 eq), carboxylic acid **24** (25 mg, 0.11 mmol, 1.2 eq) and 2-chloro-1-methylpyridinium

iodide (28 mg, 0.11 mmol, 1.2 eq) in DCM at 0 °C under argon atmosphere, was added DIPEA (52 µl, 0.29 mmol, 3 eq). The reaction mixture was allowed to warm to r.t. and stirred. After 4-24h (check by TLC), water was added, and the layers were separate. The aqueous layer was extracted with DCM. The combined organic layers were dried over Na₂SO₄ and concentrated in vacuo. The crude was purified by flash chromatography with isocratic gradient (hexane: AcOEt; 100:0→0:100) to afford the title compound (**49**) as an orange solid. (22 mg, 52 %). m.p. 149 °C. ¹H NMR (400 MHz, CDCl₃): δ = 8.35 – 8.28 (m, 1H), 7.35 – 7.23 (m, 4H), 7.21 – 7.09 (m, 3H), 6.96 (dt, *J* = 7.9, 1.4 Hz, 2H), 6.94 – 6.87 (m, 2H), 6.56 (s, 1H), 5.13 – 4.70 (m, 2H), 4.50 – 4.29 (m, 2H), 3.94 (s, 2H), 1.73 – 1.54 (m, 4H), 1.21 (d, *J* = 15.2 Hz, 2H). ¹³C NMR (101 MHz, CDCl₃): δ = 165.7 (1C), 155.7 (1C), 153.5 (1C), 135.6 (1C), 131.6 (1C), 130.6 (1C), 130.4 (1C), 130.1 (1C), 128.8 (1C), 128.4 (1C), 128.2 (1C), 128.1 (1C), 127.9 (1C), 124.2 (1C), 122.8 (1C), 122.4 (1C), 121.6 (1C), 119.2 (1C), 119.1 (1C), 109.5 (1C), 109.2 (1C), 83.7 (1C), 53.0 (1C), 46.6 (1C), 30.0 (1C), 29.4 (1C), 22.8 (1C). *t_R* (min) = 9.51 (*Z*) + 10.44 (*E*), purity = 99.5%. MS: *m/z* [M+H]⁺ calc. for (C₂₇H₂₅FN₄O)⁺ = 441.21, found 441.20. High-Resolution Mass: *m/z* calcd for C₂₇H₂₅FN₄NaO, 463.1905; found, 463.1908.

Biological Assays. Radioligand Binding Assay. For the experiments, hCB₂-HEK cells were a gift from AbbVie Laboratories (Chicago, USA). Cells were grown in Dulbecco's modified Eagle's medium containing high glucose supplemented with 10 % fetal calve serum (FCS), penicillin / streptomycin (100 U / mL / 100 µg / mL) and 25 µg/ml zeocin in a 37 °C incubator in the presence of 5% CO₂. The respective hCB₂R membranes were prepared as described in literature²⁶. The rCB₁R membrane homogenate was prepared from brains of adult female rats frozen at -80 °C^{65, 66} given from an alternate project by Prof. Kristina Lorenz of the Institute of Pharmacology and Toxicology at the University of Würzburg. The respective rCB₁R membranes were freshly prepared according to the protocol described by Catani and Gasperi for preparation of membrane homogenates⁶⁷.

CBRs saturation and competition assays were performed according to protocols previously established in the M. Decker research group^{26, 30}. For the determination of K_D value of the membrane samples, saturation assays were done taking 8 concentrations of [³H] CP55940 (Hartmann Analytic GmbH) ranging from 0.1 nM to 5.0 nM. Reactions were started by adding membrane (12.5 µg/well for rCB₁ or 8 µg/well for hCB₂) of a 96 well Multiscreen filter plate (Millipore) containing the radioligand in assay buffer (50 mM Tris-HCl, pH = 7.4; 5 mM MgCl₂ x 6 H₂O; 2.5 mM EDTA). After 3 h incubation at 37°C, the reaction was stopped by vacuum filtration and each well was washed 4 times with cold binding buffer (50 mM Tris-HCl, pH = 7.4; 5 mM MgCl₂ x 6 H₂O; 2.5 mM EDTA). The filter plate was dried at 45 °C. After cooling to ambient temperature, 20 µL IRGA Safe plus-scintillation cocktail (Perkin Elmer) were added to each well. The activity was counted in a MicroBeta TriLux-Counter (Wallac - PerkinElmer). Competition assays were done with 7 concentrations (0.10 nM – 0.32 mM) of target compound (previously isomerized to their *cis* or *trans* states with light at different wavelengths according to the nature of each compound) and 0.62 nM [³H] CP55940. The positive controls for

the assays over rCB₁ and hCB₂ were the respective the selective ligands rimonabant and reference compound **52** (both synthesized in house).

The stock solutions of all tested compounds (5 mM) were prepared as solution in DMSO. The dilution rows of all compound stock solutions were prepared in binding buffer.

Statistical analyses and sigmoidal dose-response curve fittings were performed with GraphPad Prism 6 for Windows (v. 6.01, September 21, 2012). K_i values were determined according to the Cheng-Prusoff equation:

$$K_i = \frac{EC_{50}}{1 + \frac{[L^*]}{K_D}}$$

with [L*] as radioligand concentration. The K_i values were calculated of at least two individual experiments. K_D values were measured in at least two individual experiments for each new batch of prepared membrane.

Internalization of CB₁R by flow cytometry. The cDNA of the hCB₁R was obtained from the cDNA resource center (www.cdna.org). PCR was used to delete amino acids 1-25 (as previously described in the literature)⁶⁸ and create homology sequence with the signal-sequence-Flag vector.⁶⁹ The cDNA of the hCB₂R was a generous gift from Dr Guillermo Yudowski, University of Puerto Rico, and PCR was used to amplify the full receptor. NEBuilder was then used to create the final SS-Flag-CB₁R and SS-Flag-CB₂R. Stable cell lines were created by transfecting HEK293 cells and selecting with Zeocin. Resistant colonies were selected and screened for expression by fluorescent microscopy using anti-Flag M1 (Sigma) conjugated with AlexFluor -647 (ThermoFisher). Internalization was measured using a previously described assay.⁴⁹ Briefly, Flag-tagged surface receptors were labelled with the calcium sensitive antibody anti-FlagM1 conjugated to AlexaFluor647 for 30 min at 37°C. Compound dilutions were prepared in DMSO and irradiated with the respective wavelength for 5 min before addition to the wells and were incubated for 45 min at 37°C (containing 0.2 % DMSO). For testing compounds in antagonist mode, receptors were stimulated by simultaneously adding the agonist CP55940 (**2**) in a fixed concentration of 10 nM with the respective test compound dilutions. Following stimulation, cells were rapidly washed with PBS/EDTA (0.04 %) to remove any surface antibody. Cells were suspended in PBS/EDTA (0.04 %), pelleted (1100 rpm, 4°C, 5 min) and resuspended in PBS (containing Ca²⁺) to measure endocytosis. The increase in fluorescence due to previous internalization of the fluorescent tagged receptors was analyzed using a FACSCalibur (BD Biosciences) with 5000 events being analyzed in all cases. The data was analyzed from at least three independent experiments using sigmoidal dose-response curve fitting in GraphPad Prism 6 for Windows (v. 6.01, September 21, 2012).

Fluorescence-based measurement of GRABeCB_{2.0} activation. HEK293T cells were cultured in Dulbecco's modified eagle's medium (DMEM) (PAN Biotech) supplemented with 10% (vol/vol) fetal bovine serum (FBS) (Biochrom AG), 2 mM L-glutamine, and penicillin/streptomycin (100 U/mL / 100 µg/mL). Cells were maintained at 37°C and 5% CO₂ in a humidified atmosphere. Cells were routinely passaged by aspirating the medium, washing with phosphate-buffered

saline (PBS) (Sigma-Aldrich), de-attaching with trypsin 0.05%/(ethylenedinitrilo)tetraacetic acid 0.02% in PBS and resuspending in culture DMEM. To perform the assays, 2 million HEK293T cells were seeded in 10-cm cell culture dishes. After 24 hours, cells were transfected with 2 μ g GRABeCB2.0-containing plasmid DNA using the jetPRIME reagent according to the manufacturer's protocol. Later, 24 hours after transfection, cells were resuspended in culture DMEM and seeded into a black-walled, black-bottom 96-well plate, at a density of 50,000 cells per well. Prior to performing the assay, photoswitchable ligands were isomerized under LED light (CoolLED pE-4000) at $\lambda = 365$ nm (*cis*) or $\lambda = 450$ nm (*trans*) for 10 minutes. After isomerization, ligand dilution series were prepared under dark conditions. After 24 hours, cells were washed with PBS, and then 90 μ L of prewarmed PBS was added to each well. After 5 minutes of incubation at 37 °C, fluorescence was measured at 37 °C using a Synergy Neo2 Plate Reader (Biotek) using an excitation wavelength of 479/20 nm and emission window of 520/20 nm (detector gain: 120V). Each well was measured once before and after treatment with 10 μ L volume of ligands at different concentrations. Fluorescence change upon ligand treatment was calculated using the following formula:

$$\Delta F = (F_{\text{post}} - F_{\text{pre}} / F_{\text{pre}}) * 100$$

where F_{pre} is the measured fluorescence value before ligand stimulus and F_{post} is the fluorescence after stimulus. For each ligand concentration 4 to 8 wells were measured per plate and responses were averaged. For the statistical analysis, each data point and error bar represent the average of 3-7 independent experiments \pm standard error of the mean (SEM). Data was fit to Hill equation with variable slope to obtain the EC_{50} values using GraphPad Prism Prism 6 for Windows (v. 6.01, September 21, 2012).

hCB Calcium Mobilization Assay. Chinese hamster ovarian (CHO-K1) cells stably expressing $G\alpha q16$ with either *hCB*₁ or *hCB*₂ receptor were cultivated in Ham's nutrient mixture F12 (Merck) supplemented with 10 % FCS and penicillin/streptomycin (90 U/mL / 90 μ g/mL). *hCB*₁ cells were selected using hygromycin (200 μ g/mL) and geneticin (400 μ g/mL). Zeocin (200 μ g/mL) and hygromycin (200 μ g/mL) were used for the selection of *hCB*₂. Cells were plated onto 96-well plates (30,000 cells/well) to a final volume of 100 μ L/well and incubated at 37 °C for 24 h. Cells were washed with freshly prepared assay buffer made up from 10 x Hanks' balanced salt solution (HBSS, containing final concentrations of 137.0 mM NaCl, 5.4 mM KCl, 1.3 mM CaCl₂, 0.4 mM MgSO₄, 0.5 mM MgCl₂, 0.3 mM Na₂HPO₄, 0.4 mM KH₂PO₄, 4.2 mM NaHCO₃ and 5.6 mM D-glucose), 1M HEPES (final concentration 20 mM), bovine serum albumin (1%) and Probenecid (dissolved in 1 M NaOH, final concentration 2.7 mM) adjusted to pH 7.4. Cells were loaded with 100 μ L Fluo-4 AM (4 μ M) at 37 °C for 1 h. The dye was removed and 60 μ L of assay buffer (100 μ L for controls) was added to the dye-loaded cells. Calcium flux was monitored using an automated plate reader (FlexStation 3, Molecular devices) at an excitation wavelength of 495 nm and an emission wavelength of 525 nm. Test compounds were irradiated with the wavelength of interest for 10 min directly before addition. After measuring the baseline for 15 sec, test compounds in assay buffer (< 0.5 % DMSO) with various concentrations,

compound CP55940 (positive control) or DMSO (negative control) was added automatically, and fluorescence was monitored for 5 min. All experiments were performed in duplicates in three independent experiments. EC_{50} values were analyzed from the respective area under curve with sigmoidal dose-response curve fitting using GraphPad Prism Prism 9 for Windows (v. 6.01, September 21, 2012).

Analysis of ERK1/2 activation by Western Blot. CHO cells expressing $G\alpha q16$ and *hCB*₁ were plated in 6 well plates (1*10⁶ cells/well) for 24 h and starved for another 24h in serum free media. Test compounds were irradiated with the wavelength of interest for 5 min. Cells were stimulated for 15 min with the indicated compounds and lysed using an ice-cold lysis buffer (1% (V/V) Triton-X-100, 5 mM EDTA, 300 mM NaCl, 50 mM Tris (pH 7.4), 20 μ g/mL soybean trypsin inhibitor, 0.4 mM benzamidine, 1 mM PMSF, 50 mM NaF, 5 mM Na₄P₃O₇, 1 mM Na₃VO₄, and 1.5 mM NaN₃). After 10 min (4 °C), sonification was performed and the lysates were centrifuged (20,000 g, 15 min). The colorimetric BCA protein Assay Kit (ThermoScientific) was used to determine the protein concentration. Equal amounts of protein per sample were separated using SDS/PAGE. After the transfer to a PVDF membrane (Amersham; Hybond-P), the membranes were blocked with 5 % (w/V) fat-free milk dissolved in Tris-buffered saline with 0.1 % (V/V) Tween-20 or 5 % (w/V) BSA dissolved in Tris-buffered saline with 0.2 % (V/V) NP-40 for 1 h at room temperature. The membranes were incubated with the indicated primary antibodies over night at 4 °C. Following primary antibodies were used: phosphoERK1/2(TEY) (1:1,000; no.9101L, Cell Signaling), ERK1/2 (1:1,000; no. 9102, Cell Signaling). A horseradish-peroxidase-linked antibody was used as secondary antibody (1:10,000; no. 111-035-144). Membrane bound antibodies were detected using a luminol solution (125 mM luminol, 45 mM coumaric acid, TRIS 1 M (pH 8.3), 0.015 % (V/V) H₂O₂). Data analysis was performed with ImageJ and GraphPad Prism 9 for Windows (v. 9.3.1).

NanoBiT® β arr2 recruitment assays. CBR activation potential was evaluated using live cell NanoBiT® assays, following the recruitment of β arr2 to the receptor upon activation. The NanoLuc Binary Technology, developed by Promega, is based on functional complementation of a split nanoluciferase. The establishment of the used assays has been described before.⁷⁰⁻⁷² HEK293T cells stably expressing either the *CB*₁- β arr2 or *CB*₂- β arr2 reporter system were routinely maintained at 37 °C, 5% CO₂, under humidified atmosphere in Dulbecco's modified Eagles medium (Gluta-Max™) (DMEM) supplemented with 10% heat-inactivated fetal bovine serum (FBS), 100 IU/mL of penicillin, 100 μ g/mL of streptomycin and 0.25 μ g/mL of amphotericin B. On the day prior to experiments, cells were seeded in white 96-well plates, coated with poly-D-lysine, and incubated overnight. Stock solutions were made by dissolving compound **27a** in DMSO and working solutions were made by serial dilution in Opti-Mem I Reduced Serum and MeOH (50/50 % v/v), resulting in an in well DMSO concentration of 0.09 %. The next day, cells were rinsed twice with 150 μ L of Opti-MEM, after which 100 μ L of this assay medium was added to each well. Subsequently, 25 μ L of the 20-fold diluted Nano-Glo® Live Cell reagent, containing the cell-permeable furimazine substrate was added and the plate

was placed into a TriStar² LB 942 Multimode Microplate Reader (Berthold Technologies GmbH & Co., Germany). Luminescence was measured for 10-15 min until the signal stabilized. To evaluate CB activity of the 2 photo-isomers of **27a**, 13.5x concentrated stock solutions were either irradiated with $\lambda = 365$ nm (cis) or $\lambda = 450$ nm (trans) for 5 min and added to the cells. Luminescence was then monitored for 2 hours. A concentration range of reference standard CP55940, as well as appropriate solvent controls were present on each plate. To assess dynamic photomodulation of **27a**, 3 high concentrations (10 μ M, 1 μ M and 100 nM) were prepared as described previously. Stock solutions then were subjected to 1, 2, 3 or 4 irradiations, switching between **27a-cis** and **27a-trans**. Stock solutions were added to the cells and the assay was performed as mentioned above. Raw data were initially processed using Microsoft Excel 2019. Luminescence values were baseline-corrected for inter-well variability and a blank correction was performed by subtracting the area under the curve (AUC) values of the solvent controls. Using the GraphPad Prism software (Version 9.3.0) (San Diego, CA, USA), concentration-response curves were obtained by normalizing to the Emax of the reference standard CP55940, set at 100%. Curve fitting of the concentration-response curves via nonlinear regression (three-parameter logistic fit) was performed to obtain EC50 (potency) and Emax values (efficacy).

Molecular Docking. The 2D structures of the compounds were drawn with ChemDraw (v. 18.0, PerkinElmer) and MarvinSketch for Windows (v. 19.10.0, ChemAxon Ltd.). Docking experiments were performed as previously described³⁰. The crystal structure of the agonist bound hCB₁R (PDB ID: 5XRA) was prepared using MOE⁷³ (version 2016.08). MOE's protein structure preparation pipeline⁷⁴⁻⁷⁹ was used to remove ligands and water molecules, followed by automatic assignment of tautomer and protonation states using Protonate3D⁸⁰ at pH 7.5. Geometry optimization of AM11542, reference compound **4** and target compounds **27a** and **28a** was performed using the MMFF94x^{81, 82} force field (gradient convergence criterion: 0.001 RMS·kcal·mol⁻¹·Å⁻¹). Pose reproduction performance was assessed by RMSD between docked poses and the experimental binding pose of AM11542 (PDB ID: 5XRA).

The GOLD program (v5.4.1) was used to dock the ligands under default settings. The knowledge-based scoring function ASP was found to robustly model experimentally observed intermolecular interactions of AM11542 and to yield the best crystal pose reproduction among all of GOLD's scoring functions (RMSD of 0.47 Å for the top ranked pose).

The 50 best ASP poses of each ligand were rescored using the knowledge-based scoring function DSX (v0.89), with CSD and PDB potentials (version 05/11). Compound **4** and the *cis* and *trans* isomers of compound **27a**, and compound **28a-cis** were manually prepared in MOE's Builder tool and subsequently prepared and evaluated under the same conditions as for AM11542.

To reliably compare the docking scores of molecules with different molecular sizes, the original ASP scores were normalized by the cubic root of the heavy atom count of each ligand (cubic root score),⁶¹ as defined by the expression:

$$CRS = Score * \frac{1}{\sqrt[3]{Heavy\ atom\ number}}$$

ASSOCIATED CONTENT

The supporting information is available free of charge via the Internet at <http://pubs.acs.org>.

The document contains: HPLC chromatogram of target compounds, molecular docking and scoring, photostationary distribution (compounds **27a** and **49**), ¹H-NMR and ¹³C-NMR spectra of target compounds, thermal stability graphics of target compounds, supplementary figures of biological assays, and process for the synthesis of selected intermediates.

AUTHOR INFORMATION

Corresponding Author

* **Michael Decker** - Pharmaceutical and Medicinal Chemistry, Institute of Pharmacy and Food Chemistry, Julius Maximilian University of Würzburg, Am Hubland 97074, Würzburg, Germany; orcid.org/0000-0002-6773-6245; Phone: +49 931 3189676; Email: michael.decker@uni-wuerzburg.de

Author Contributions

M. Decker was responsible for the supervision and development of the whole project. D. A. Rodríguez-Soacha performed the chemical synthesis, testing of the physicochemical properties of the target compounds and performing the radioligand binding assays. Additional radioligand binding experiments were done by S. A. M. Steinmüller. Western Blots were obtained by J. Fender under the supervision of K. Lorenz. M. H. Deventer performed β arr2 assays (NanoBiT®) and dynamic photomodulation experiments under the supervision of C. P. Stove. The calcium mobilization assay was established with the help of J. Fender under supervision of K. Lorenz, and the experiments were performed by S. A. M. Steinmüller and A. Tutov. Computational docking studies were performed by Y. Ramírez with supervision by C. Sotriffer. A. Işbilir with supervision by M. J. Lohse performed fluorescence biosensor-based receptor activation assays. The flow cytometry analysis of internalization was performed by S. A. M. Steinmüller under supervision of J. N. Hislop. All authors have given approval to the final version of the manuscript.

Funding Sources

This project was financially supported by the German Research Foundation (Deutsche Forschungsgemeinschaft under DFG DE1546/10-1) and a Ph.D. scholarship for D. A. Rodríguez-Soacha by the German Academic Exchange Service (Deutscher Akademischer Austauschdienst. DAAD). Y. Ramírez was granted a scholarship by the DAAD program "Research stays for university academics and scientists". A. Tutov and J. Fender were supported by the International Doctoral Program funded within the framework of the Elite Network of Bavaria (grant N° K-BM-2013-247). J. N. Hislop financing support was given by NHS Grampian. The research visit of S. A. M. Steinmüller in J. N. Hislop's laboratory was also funded by the Elite Network of Bavaria (grant N° K-BM-2013-247). M. H. Deventer was supported by the Research Foundation Flanders (FWO, grant number 1S54521N).

Notes

The authors declare no competing financial interest.

ACKNOWLEDGMENT

Special thanks to Dr. Rangan Maitra and RTI International for providing the $G\alpha q16$ coupled hCB_1 and hCB_2 CHO-K1 cell lines. We thank Nadine Yurdagül-Hemmerich for excellent technical support.

ABBREVIATIONS

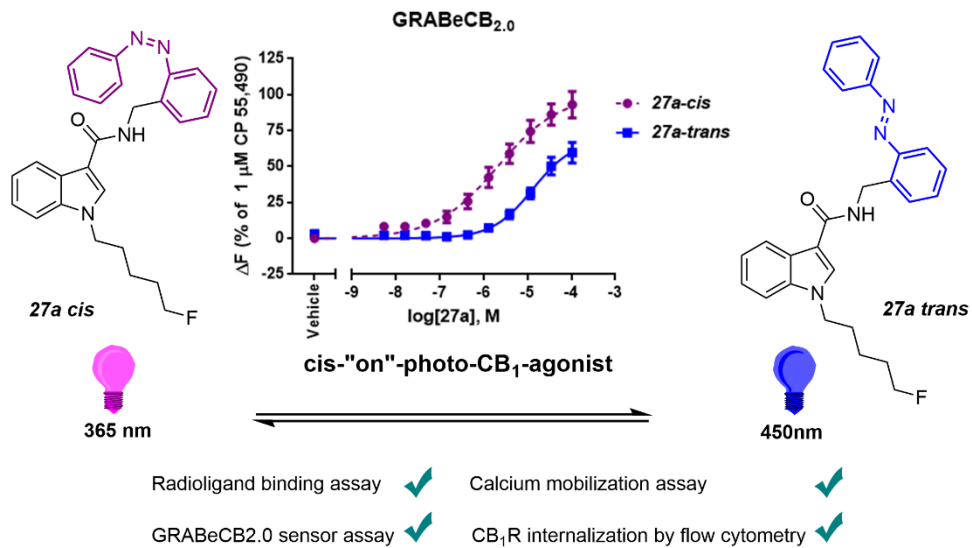
hCB_1R , human cannabinoid receptor 1; hCB_2R , human cannabinoid receptor 2; rCB_1R , rat cannabinoid receptor 1; Boc₂O, Di-*tert*-butyl decarbonate; DCM, dichloromethane; DIPEA, *N,N*-Diisopropylethylamine; *mCPBA*, *meta*-chloroperbenzoic acid; MPS, potassium peroxymonosulfate; PPh₃, triphenylphosphine; TEA, triethylamine; TFA, trifluoroacetic acid; TLC, thin layer chromatography; TMS-acetylene, trimethylsilylacetylene.

REFERENCES

1. Gaoni, Y., and Mechoulam, R. (1964) Isolation, Structure, and Partial Synthesis of an Active Constituent of Hashish. *J. Am. Chem. Soc.* 86 (8), 1646-1647.
2. Zou, S., and Kumar, U. (2018) Cannabinoid Receptors and the Endocannabinoid System: Signaling and Function in the Central Nervous System. *Int. J. Mol. Sci.* 19 (3), 833.
3. Sviženská, I., Dubový, P., and Šulcová, A. (2008) Cannabinoid receptors 1 and 2 (CB1 and CB2), their distribution, ligands and functional involvement in nervous system structures — A short review. *Pharmacol. Biochem. Behav.* 90 (4), 501-511.
4. Howlett, A. C., and Abood, M. E. (2017) CB(1) and CB(2) Receptor Pharmacology. *Adv. Pharmacol.* 80, 169-206.
5. Mackie, K. (2005) Distribution of Cannabinoid Receptors in the Central and Peripheral Nervous System. In *Cannabinoids* (Pertwee, R. G., Ed.) pp 299-325, Springer, Berlin.
6. Haller, J., Varga, B., Ledent, C., and Freund, T. F. (2004) CB1 cannabinoid receptors mediate anxiolytic effects: convergent genetic and pharmacological evidence with CB1-specific agents. *Behav. Pharmacol.* 15 (4), 299-304.
7. Shen, C.-J., Zheng, D., Li, K.-X., Yang, J.-M., Pan, H.-Q., Yu, X.-D., Fu, J.-Y., Zhu, Y., Sun, Q.-X., Tang, M.-Y., Zhang, Y., Sun, P., Xie, Y., Duan, S., Hu, H., and Li, X.-M. (2019) Cannabinoid CB1 receptors in the amygdalar cholecystokinin glutamatergic afferents to nucleus accumbens modulate depressive-like behavior. *Nat. Med.* 25 (2), 337-349.
8. Rosenberg, E. C., Tsien, R. W., Whalley, B. J., and Devinsky, O. (2015) Cannabinoids and Epilepsy. *Neurotherapeutics* 12 (4), 747-768.
9. Darmani, N. A. (2010) Mechanisms of Broad-Spectrum Antiemetic Efficacy of Cannabinoids against Chemotherapy-Induced Acute and Delayed Vomiting. *Pharmaceuticals* 3 (9), 2930-2955.
10. Murphy, T., and Le Foll, B. (2020) Targeting the Endocannabinoid CB1 Receptor to Treat Body Weight Disorders: A Preclinical and Clinical Review of the Therapeutic Potential of Past and Present CB1 Drugs. *Biomolecules* 10 (6), 855.
11. O'Sullivan, S. E., Yates, A. S., and Porter, R. K. (2021) The Peripheral Cannabinoid Receptor Type 1 (CB1) as a Molecular Target for Modulating Body Weight in Man. *Molecules* 26 (20), 6178.
12. Sansone, R. A., and Sansone, L. A. (2014) Marijuana and body weight. *Innov. Clin. Neurosci.* 11 (7-8), 50-54.
13. Woodhams, S. G., Chapman, V., Finn, D. P., Hohmann, A. G., and Neugebauer, V. (2017) The cannabinoid system and pain. *Neuropharmacology* 124, 105-120.
14. Worob, A., and Wenthur, C. (2020) DARK Classics in Chemical Neuroscience: Synthetic Cannabinoids (Spice/K2). *ACS Chem. Neurosci.* 11 (23), 3881-3892.
15. Spaderna, M., Addy, P. H., and D'Souza, D. C. (2013) Spicing things up: synthetic cannabinoids. *Psychopharmacology* 228 (4), 525-540.
16. Schifano, F., Orsolini, L., Papanti, D., and Corkery, J. (2017) NPS: Medical Consequences Associated with Their Intake. In *Neuropharmacology of New Psychoactive Substances (NPS): The Science Behind the Headlines* (Baumann, M. H., Glennon, R. A., and Wiley, J. L., Eds.) pp 351-380, Springer, Cham.
17. Krämer, J., Kang, R., Grimm, L. M., De Cola, L., Picchetti, P., and Biedermann, F. (2022) Molecular Probes, Chemosensors, and Nanosensors for Optical Detection of Biorelevant Molecules and Ions in Aqueous Media and Biofluids. *Chem. Rev.* 122 (3), 3459-3636.
18. Linsley, C. S., and Wu, B. M. (2017) Recent advances in light-responsive on-demand drug-delivery systems. *Ther. Deliv.* 8 (2), 89-107.
19. Lerch, M. M., Hansen, M. J., and van Dam, G. M. Szymanski, W., and Feringa, B. L. (2016) Emerging Targets in Photopharmacology. *Angew. Chem., Int. Ed.* 55 (37), 10978-10999. (2016) *Angew. Chem.* 128 (37), 11140-11163.
20. Paoletti, P., Ellis-Davies, G. C. R., and Mouro, A. (2019) Optical control of neuronal ion channels and receptors. *Nat. Rev. Neurosci.* 20 (9), 514-532.
21. Ricart-Ortega, M., Font, J., and Llebaria, A. (2019) GPCR photopharmacology. *Mol. Cell. Endocrinol.* 488, 36-51.
22. Rodríguez-Soacha, D. A., and Decker, M. (2018) Photopharmacology in Alzheimer's Disease. *Adv. Ther.* 1 (3), 1800037.
23. Mehta, Z. B., Johnston, N. R., Nguyen-Tu, M.-S., Broichhagen, J., Schultz, P., Larner, D. P., Leclerc, I., Trauner, D., Rutter, G. A., and Hodson, D. J. (2017) Remote control of glucose homeostasis in vivo using photopharmacology. *Sci. Rep.* 7 (1), 291-291.
24. Westphal, M. V., Schafroth, M. A., Sarott, R. C., Imhof, M. A., Bold, C. P., Leippe, P., Dhopeshwarkar, A., Grandner, J. M., Katritch, V., Mackie, K., Trauner, D., Carreira, E. M., and Frank, J. A. (2017) Synthesis of Photoswitchable Δ^9 -Tetrahydrocannabinol Derivatives Enables Optical Control of Cannabinoid Receptor 1 Signaling. *J. Am. Chem. Soc.* 139 (50), 18206-18212.
25. Watkins, A. R. (2019) Cannabinoid interactions with ion channels and receptors. *Channels* 13 (1), 162-167.
26. Dolles, D., Strasser, A., Wittmann, H.-J., Marinelli, O., Nabissi, M., Pertwee, R. G., and Decker, M. (2018) The First Photochromic Affinity Switch for the Human Cannabinoid Receptor 2. *Adv. Ther.* 1 (1), 1700032.
27. Westphal, M. V., Sarott, R. C., Zirwes, E. A., Osterwald, A., Guba, W., Ullmer, C., Grether, U., and Carreira, E. M. (2020) Highly Selective, Amine-Derived Cannabinoid Receptor 2 Probes. *Chem. Eur. J.* 26 (6), 1380-1387.
28. Sarott, R. C., Viray, A. E. G., Pfaff, P., Sadybekov, A., Rajic, G., Katritch, V., Carreira, E. M., and Frank, J. A. (2021) Optical Control of Cannabinoid Receptor 2-Mediated Ca²⁺ Release Enabled by Synthesis of Photoswitchable Probes. *J. Am. Chem. Soc.* 143 (2), 736-743.
29. Hu, T., Zheng, G., Xue, D., Zhao, S., Li, F., Zhou, F., Zhao, F., Xie, L., Tian, C., Hua, T., Zhao, S., Xu, Y., Zhong, G., Liu, Z.-J., Makriyannis, A., Stevens, R. C., and Tao, H. (2021) Rational Remodeling of Atypical Scaffolds for the Design of Photoswitchable Cannabinoid Receptor Tools. *J. Med. Chem.* 64 (18), 13752-13765.
30. Rodríguez-Soacha, D. A., Fender, J., Ramírez, Y. A., Collado, J. A., Muñoz, E., Maitra, R., Sotriffer, C., Lorenz, K., and Decker, M. (2021) "Photo-Rimonabant": Synthesis and Biological Evaluation of Novel Photoswitchable Molecules Derived from Rimonabant Lead to a Highly Selective and Nanomolar "Cis-On" CB1R Antagonist. *ACS Chem. Neurosci.* 12 (9), 1632-1647.
31. Makriyannis, A. D., Hongfeng, D., (2000) Cannabimimetic indole derivatives. US Patent 7241799B2.
32. Hess, C., Schoeder, C. T., Pillaiyar, T., Madea, B., and Müller, C. E. (2016) Pharmacological evaluation of synthetic

- cannabinoids identified as constituents of spice. *Forensic. Toxicol.* **34**, 329-343.
33. Ametovski, A., Macdonald, C., Manning, J. J., Haneef, S. A. S., Santiago, M., Martin, L., Sparkes, E., Reckers, A., Gerona, R. R., Connor, M., Glass, M., and Banister, S. D. (2020) Exploring Stereochemical and Conformational Requirements at Cannabinoid Receptors for Synthetic Cannabinoids Related to SDB-006, 5F-SDB-006, CUMYL-PICA, and 5F-CUMYL-PICA. *ACS Chem. Neurosci.* **11** (21), 3672-3682.
 34. Banister, S. D., Moir, M., Stuart, J., Kevin, R. C., Wood, K. E., Longworth, M., Wilkinson, S. M., Beinat, C., Buchanan, A. S., Glass, M., Connor, M., McGregor, I. S., and Kassiou, M. (2015) Pharmacology of Indole and Indazole Synthetic Cannabinoid Designer Drugs AB-FUBINACA, ADB-FUBINACA, AB-PINACA, ADB-PINACA, 5F-AB-PINACA, 5F-ADB-PINACA, ADBICA, and 5F-ADBICA. *ACS Chem. Neurosci.* **6** (9), 1546-1559.
 35. Seo, H. J., Kim, M. J., Lee, S. H., Lee, S.-H., Jung, M. E., Kim, M.-S., Ahn, K., Kim, J., and Lee, J. (2010) Synthesis and structure-activity relationship of 1,2,4-triazole-containing diarylpyrazolyl carboxamide as CB1 cannabinoid receptor-ligand. *Bioorg. Med. Chem.* **18** (3), 1149-1162.
 36. Hamon, F., Djedaini-Pilard, F., Barbot, F. and Len, C. (2009) Azobenzenes—synthesis and carbohydrate applications. *Tetrahedron* **65** (49), 10105-10123.
 37. Merino, E. (2011) Synthesis of azobenzenes: the coloured pieces of molecular materials. *Chem. Soc. Rev.* **40** (7), 3835-3853.
 38. Calbo, J., Thawani, A. R., Gibson, R. S. L., White, A. J. P., and Fuchter, M. J. (2019) A combinatorial approach to improving the performance of azoarene photoswitches. *Beilstein J. Org. Chem.* **15**, 2753-2764.
 39. Maier, M. S., Hüll, K., Reynders, M., Matsuura, B. S., Leippe, P., Ko, T., Schäffer, L., and Trauner, D. (2019) Oxidative Approach Enables Efficient Access to Cyclic Azobenzenes. *J. Am. Chem. Soc.* **141** (43), 17295-17304.
 40. Schehr, M., Hugenbusch, D., Moje, T., Näther, C., and Herges, R. (2018) Synthesis of mono-functionalized S-diazocines via intramolecular Baeyer-Mills reactions. *Beilstein J. Org. Chem.* **14**, 2799-2804.
 41. Lentes, P., Stadler, E., Röhricht, F., Brahms, A., Gröbner, J., Sönnichsen, F. D., Gescheidt, G., and Herges, R. (2019) Nitrogen Bridged Diazocines: Photochromes Switching within the Near-Infrared Region with High Quantum Yields in Organic Solvents and in Water. *J. Am. Chem. Soc.* **141** (34), 13592-13600.
 42. Cabré, G., Garrido-Charles, A., González-Lafont, À., Moormann, W., Langbehn, D., Egea, D., Lluch, J. M., Herges, R., Alibés, R., Busqué, F., Gorostiza, P., and Hernando, J. (2019) Synthetic Photoswitchable Neurotransmitters Based on Bridged Azobenzenes. *Org. Lett.* **21** (10), 3780-3784.
 43. Heintze, L., Schmidt, D., Rodat, T., Witt, L., Ewert, J., Kriegs, M., Herges, R., and Peifer, C. (2020) Photoswitchable Azo- and Diazocine-Functionalized Derivatives of the VEGFR-2 Inhibitor Axitinib. *Int. J. Mol. Sci.* **21** (23).
 44. Sanz, R., Escribano, J., Fernández, Y., Aguado, R., Pedrosa, M. R., and Arnáiz, F. J. (2005) Deoxygenation of N-Oxides with Triphenylphosphine, Catalyzed by Dichlorodioxomolybdenum(VI). *Synlett* **2005** (09), 1389-1392.
 45. Bandara, H. M. D., and Burdette, S. C. (2012) Photoisomerization in different classes of azobenzene. *Chem. Soc. Rev.* **41** (5), 1809-1825.
 46. Agnetta, L., Kauk, M., Canizal, M. C. A., Messerer, R., Holzgrabe, U., Hoffmann, C., and Decker, M. (2017) A Photoswitchable Dualsteric Ligand Controlling Receptor Efficacy. *Angew. Chem., Int. Ed.* **56** (25), 7282-7287. (2017) *Angew. Chem.* **129** (25), 7388-7393
 47. Agnetta, L., Bermudez, M., Riefolo, F., Matera, C., Claro, E., Messerer, R., Littmann, T., Wolber, G., Holzgrabe, U., and Decker, M. (2019) Fluorination of Photoswitchable Muscarinic Agonists Tunes Receptor Pharmacology and Photochromic Properties. *J. Med. Chem.* **62** (6), 3009-3020.
 48. Page, D., Balaux, E., Boisvert, L., Liu, Z., Milburn, C., Tremblay, M., Wei, Z., Woo, S., Luo, X., Cheng, Y. X., Yang, H., Srivastava, S., Zhou, F., Brown, W., Tomaszewski, M., Walpole, C., Hodzic, L., St-Onge, S., Godbout, C., Salois, D., and Payza, K. (2008) Novel benzimidazole derivatives as selective CB2 agonists. *Bioorg. Med. Chem. Lett.* **18** (13), 3695-700.
 49. Thompson, D., McArthur, S., Hislop, J. N., Flower, R. J., and Perretti, M. (2014) Identification of a novel recycling sequence in the C-tail of FPR2/ALX receptor: association with cell protection from apoptosis. *J. Biol. Chem.* **289** (52), 36166-78.
 50. Dong, A., He, K., Dudok, B., Farrell, J. S., Guan, W., Liput, D. J., Puhl, H. L., Cai, R., Wang, H., Duan, J., Albarran, E., Ding, J., Lovinger, D. M., Li, B., Soltesz, I., and Li, Y. (2021) A fluorescent sensor for spatiotemporally resolved imaging of endocannabinoid dynamics in vivo. *Nat Biotechnol.* Epub ahead of print.
 51. Ambrosio, M., and Lohse, M. J. (2012) Nonequilibrium Activation of a G-Protein-Coupled Receptor. *Mol. Pharmacol.* **81** (6), 770-777.
 52. Fulp, A., Zhang, Y., Bortoff, K., Seltzman, H., Snyder, R., Wiethel, R., Amato, G., and Maitra, R. (2016) Pyrazole antagonists of the CB1 receptor with reduced brain penetration. *Bioorg. Med. Chem.* **24** (5), 1063-1070.
 53. Galve-Roperh, I., Rueda, D., Gómez del Pulgar, T., Velasco, G., and Guzmán, M., (2002) Mechanism of Extracellular Signal-Regulated Kinase Activation by the CB1 Cannabinoid Receptor. *Mol. Pharmacol.* **62** (6), 1385-1392.
 54. Tomasovic, A., Brand, T., Schanbacher, C., Kramer, S., Hümmert, M. W., Godoy, P., Schmidt-Heck, W., Nordbeck, P., Ludwig, J., Homann, S., Wiegner, A., Shaykhutdinov, T., Kratz, C., Knüchel, R., Müller-Hermelink, H.-K., Rosenwald, A., Frey, N., Eichler, J., Dobrev, D., El-Armouche, A., Hengstler, J. G., Müller, O. J., Hinrichs, K., Cuello, F., Zernecke, A., and Lorenz, K. (2020) Interference with ERK-dimerization at the nucleocytosolic interface targets pathological ERK1/2 signaling without cardiotoxic side-effects. *Nat. Commun.* **11** (1), 1733.
 55. Mooij, W. T. M., and Verdonk, M. L. (2005) General and targeted statistical potentials for protein-ligand interactions. *Proteins* **61** (2), 272-287.
 56. Cole, J. C., Nissink, J. W. M., and Taylor, R. (2005) Protein-ligand docking and virtual screening with GOLD. In *Virtual Screening in Drug Discovery*, Vol. 1, pp 379-415, Taylor & Francis, CRC Press, Boca Raton, FL.
 57. Verdonk, M. L., Cole, J. C., Hartshorn, M. J., Murray, C. W., and Taylor, R. D. (2003) Improved protein-ligand docking using GOLD. *Proteins* **52** (4), 609-623.
 58. Hua, T., Vemuri, K., Nikas, S. P., Laprairie, R. B., Wu, Y., Qu, L., Pu, M., Korde, A., Jiang, S., Ho, J.-H., Han, G. W., Ding, K., Li, X., Liu, H., Hanson, M. A., Zhao, S., Bohn, L. M., Makriyannis, A., Stevens, R. C., and Liu, Z.-J. (2017) Crystal structures of agonist-bound human cannabinoid receptor CB1. *Nature* **547** (7664), 468-471.
 59. Kevin, R. C., Anderson, L., McGregor, I. S., Boyd, R., Manning, J. J., Glass, M., Connor, M., and Banister, S. D. (2019) CUMYL-4CN-BINACA Is an Efficacious and Potent Pro-Convulsant Synthetic Cannabinoid Receptor Agonist. *Front. Pharmacol.* **10**, 595.
 60. Neudert, G., and Klebe, G. (2011) DSX: A Knowledge-Based Scoring Function for the Assessment of Protein-Ligand Complexes. *J. Chem. Inf. Model.* **51** (10), 2731-2745.
 61. Jacobsson, M., and Karlén, A. (2006) Ligand Bias of Scoring Functions in Structure-Based Virtual Screening. *J. Chem. Inf. Model.* **46** (3), 1334-1343.
 62. Citti, C., Linciano, P., Russo, F., Luongo, L., Iannotta, M., Maione, S., Laganà, A., Capriotti, A. L., Forni, F., Vandelli, M. A., Gigli, G., and Cannazza, G. (2019) A novel phytocannabinoid isolated from *Cannabis sativa* L. with an in vivo cannabimimetic

- activity higher than Δ^9 -tetrahydrocannabinol: Δ^9 -Tetrahydrocannabiphorol. *Sci. Rep.* 9 (1), 20335.
63. Morstein, J., Romano, G., Hetzler, B., Plante, A., Haake, C., Levitz, J., and Trauner, D. (2022) Photoswitchable Serotonins for Optical Control of the 5-HT_{2A} Receptor. *Angew. Chem., Int. Ed.* e202117094.
64. Scheiner, M., Sink, A., Hoffmann, M., Vrigneau, C., Endres, E., Carles, A., Sotriffer, C., Maurice, T., and Decker, M. (2022) Photoswitchable Pseudoirreversible Butyrylcholinesterase Inhibitors Allow Optical Control of Inhibition in Vitro and Enable Restoration of Cognition in an Alzheimer's Disease Mouse Model upon Irradiation. *J. Am. Chem. Soc.* 144 (7), 3279-3284.
65. Rinaldi-Carmona, M., Barth, F., Heaulme, M., Shire, D., Calandra, B., Congy, C., Martinez, S., Maruani, J., Neliat, G., Caput, D., Ferrara, P., Soubri, P., Brelike, J. C., and Le Fur, G. (1994) SR141716A, a potent and selective antagonist of the brain cannabinoid receptor. *FEBS Lett.* 350 (2-3), 240-244.
66. Devane, W. A., Dysarz, F. A., R., J. M., Melvin, L. S., and Howlett, A. C. (1988) Determination and characterization of a cannabinoid receptor in rat brain. *Mol. Pharmacol.* 34 (5), 605-613.
67. Catani, V. M., and Gasperi, V. (2016) Assay of CB1 Receptor Binding. In *Endocannabinoid Signaling: Methods and Protocols* (Maccarrone, M., Ed.) pp 41-55, Springer New York, New York, NY.
68. McDonald, N. A., Henstridge, C. M., Connolly, C. N., and Irving, A. J. (2007) Generation and functional characterization of fluorescent, N-terminally tagged CB1 receptor chimeras for live-cell imaging. *Mol. Cell. Neurosci.* 35 (2), 237-248.
69. Zenko, D., Thompson, D., and Hislop, J. N. (2020) Endocytic sorting and downregulation of the M2 acetylcholine receptor is regulated by ubiquitin and the ESCRT complex. *Neuropharmacology* 162, 107828.
70. Cannaert, A., Storme, J., Franz, F., Auwärter, V., and Stove, C. P. (2016) Detection and Activity Profiling of Synthetic Cannabinoids and Their Metabolites with a Newly Developed Bioassay. *Anal. Chem.* 88 (23), 11476-11485.
71. Cannaert, A., Franz, F., Auwärter, V., and Stove, C. P. (2017) Activity-Based Detection of Consumption of Synthetic Cannabinoids in Authentic Urine Samples Using a Stable Cannabinoid Reporter System. *Anal. Chem.* 89 (17), 9527-9536.
72. Cannaert, A., Storme, J., Hess, C., Auwärter, V., Wille, S. M. R., and Stove, C. P. (2018) Activity-Based Detection of Cannabinoids in Serum and Plasma Samples. *Clin. Chem.* 64 (6), 918-926.
73. Chemical Computing Group ULC. (2016) *Molecular Operating Environment (MOE)*, version 2016.08, Chemical Computing Group, 1010 Sherbrooke Street West, Suite No. 910, Montreal, QC, H2A 2R7, Canada.
74. Bashford, D., and Gerwert, K. (1992) Electrostatic calculations of the pK_a values of ionizable groups in bacteriorhodopsin. *J. Mol. Biol.* 224 (2), 473-486.
75. Labute, P. (2008) The generalized Born/volume integral implicit solvent model: Estimation of the free energy of hydration using London dispersion instead of atomic surface area. *J. Comput. Chem.* 29 (10), 1693-1698.
76. Looger, L. L., and Hellinga, H. W. (2001) Generalized dead-end elimination algorithms make large-scale protein side-chain structure prediction tractable: implications for protein design and structural genomics. Edited by F. E. Cohen. *J. Mol. Biol.* 307 (1), 429-445.
77. Desmet, J., Spriet, J., and Lasters, I. (2002) Fast and accurate side-chain topology and energy refinement (FASTER) as a new method for protein structure optimization. *Proteins* 48 (1), 31-43.
78. Gilson, M. K. (1993) Multiple-site titration and molecular modeling: Two rapid methods for computing energies and forces for ionizable groups in proteins. *Proteins* 15 (3), 266-282.
79. Word, J. M., Lovell, S. C., Richardson, J. S., and Richardson, D. C., (1999) Asparagine and glutamine: using hydrogen atom contacts in the choice of side-chain amide orientation. *J. Mol. Biol.* 285 (4), 1735-1747.
80. Labute, P. (2009) Protonate3D: Assignment of ionization states and hydrogen coordinates to macromolecular structures. *Proteins* 75 (1), 187-205.
81. Halgren, T. A. (1996) Merck molecular force field. I. Basis, form, scope, parameterization, and performance of MMFF94. *J. Comput. Chem.* 17 (5-6), 490-519.
82. Halgren, T. A. (1999) MMFF VII. Characterization of MMFF94, MMFF94s, and other widely available force fields for conformational energies and for intermolecular-interaction energies and geometries. *J. Comput. Chem.* 20 (7), 730-748.



For Table of Contents